Computational simulation and model of a generalized prototype of an ornamental root

(Simulación y modelo computacional de un prototipo de raíz ornamental generalizada)

Daniela Moreno Chaparro

Universidad Nacional de Colombia

Facultad de Ingeniería, Departamento de Ingeniería Mecánica y Mecatrónica.

Bogotá, Colombia

2022

Computational simulation and model of a generalized prototype of an ornamental root

(Simulación y modelo computacional de un prototipo de raíz ornamental generalizada)

Daniela Moreno Chaparro

Tesis o trabajo de investigación presentada(o) como requisito parcial para optar al título de:
Magister en Ingeniería Mecánica

Director (a):

Diego Alexander Garzón Alvarado, Ph.D.

Codirector (a):

Gustavo Vargas Silva, Ph.D.

Línea de Investigación: Mecánica computacional.

Grupo de Investigación: Mathematical Modelling and Numerical Methods (GNUM)

Universidad Nacional de Colombia

Facultad de Ingeniería, Departamento de Ingeniería Mecánica y Mecatrónica.

Bogotá, Colombia

2022

Para mis padres.

Declaración de obra original

Yo declaro lo siguiente:

He leído el Acuerdo 035 de 2003 del Consejo Académico de la Universidad Nacional. «Reglamento sobre propiedad intelectual» y la Normatividad Nacional relacionada al respeto de los derechos de autor. Esta disertación representa mi trabajo original, excepto donde he reconocido las ideas, las palabras, o materiales de otros autores.

Cuando se han presentado ideas o palabras de otros autores en esta disertación, he realizado su respectivo reconocimiento aplicando correctamente los esquemas de citas y referencias bibliográficas en el estilo requerido.

He obtenido el permiso del autor o editor para incluir cualquier material con derechos de autor (por ejemplo, tablas, figuras, instrumentos de encuesta o grandes porciones de texto).

Por último, he sometido esta disertación a la herramienta de integridad académica, definida por la universidad.

Daniela Moreno Chaparro

Fecha 22/02/2022

Fecha

Agradecimientos

La culminación de este trabajo se da en gran parte a la ayuda, compañía y constante animo que me han brindado mi familia, amigos, colegas y mentores durante todo el proceso.

Especialmente agradezco al profesor Diego Alexander Garzón quien me ha orientado como tutor en todo este proceso con paciencia y preocupación por mi formación como profesional e investigadora. Al profesor Gustavo Vargas Silva quien también me ha animado a creer en mis capacidades, por sus valiosas ayudas y recomendaciones. A mis amigos y compañeros de maestría, quienes se han mantenido al tanto de mis procesos y me han alentado a ser mejor, creer en mí y me han dado una mano cuando más lo he necesitado. A mis padres y hermanos por el constate apoyo y amor.

Finalmente agradezco a la Universidad Nacional de Colombia ya que mi paso por esta institución me ha permitido conocer a las mejores personas.

Resumen

El crecimiento de una planta sana y productiva depende del correcto desarrollo de sus raíces y del entorno que la rodea. En este contexto, el crecimiento de las raíces es crucial porque proporciona características de soporte, anclaje y alimentación. Múltiples estudios se han centrado en interpretar y comprender el comportamiento de la raíz, proporcionando diferentes clasificaciones morfológicas y topológicas de los arquetipos de raíz. Este documento propone y evalúa dos modelos computacionales para simular el crecimiento de las raíces. El primer modelo corresponde a la representación geométrica del crecimiento de raíces en el espacio 2D y 3D. En este esquema, se abordaron cuatro arquetipos de raíces comunes como lo son: adventicia, raíz primaria, napiforme y fasciculada, adicionalmente se consideraron sus tropismos. Para desarrollar el algoritmo se consideró la inspección visual de diferentes plantas de raíz como frijoles, zanahorias y orquídeas. Seguido de esto, se realizaron simulaciones computacionales para obtener los arquetipos o morfologías de raíces deseadas. Este modelo tiene un factor estocástico que proporciona una mayor versatilidad en las simulaciones, de forma similar a las raíces reales. El segundo modelo computacional utilizado es Reaction-diffusion

Root Branching (RDRB), que modela el crecimiento dinámico de raíces usando el método de elementos finitos (FEM) en 1D para las raíces y 2D para los medios de cultivo. Este modelo proporciona una descripción más detallada y compleja que el primero, considerando la reacción-difusión de las especies, representando la búsqueda bioquímica de nutrientes. Además, explica los efectos mecánicos del crecimiento de las raíces y la interacción con el medio de crecimiento. Este modelo involucra estímulos bioquímicos, biofísicos y de tropismo. Los dos modelos matemáticos/computacionales propuestos pueden representar correctamente el crecimiento de las raíces de las plantas, incorporando aspectos geométricos y características biofísicas y bioquímicas. Además, estos modelos tienen el potencial de ser adaptados para investigar otros fenómenos naturales de ramificación, como moho mucilaginoso, fracturas, sistema circulatorio, sistema respiratorio y relámpagos.

Palabras clave: Algoritmo de crecimiento, Arquitectura de raíz, Morfología de raíz, Simulación computacional, Modelo de crecimiento de plantas.

Computational simulation and model of A generalized prototype of ornamental root.

VIII

Abstract

The growth of a healthy and productive plant depends on the correct development of its roots and the surrounding environment. In this context, root growth is crucial because it provides support, anchoring, and feeding characteristics. Multiple reported studies have focused on interpreting and understanding the root behavior, providing different morphological and topological classifications of root archetypes. This document proposes and evaluates two computational models to simulate the root growth. The first model corresponds to the geometrical representation of root growth in 2D and 3D space. In this scheme, four common root archetypes were addressed and considered their tropisms: adventitious, primary root, napiform, and fasciculate. The visual inspection of different root plants such as beans, carrots, and orchids was considered to develop the algorithm. Then, computational simulations

were carried out to obtain the desired root archetypes or morphologies. This model has a stochastic factor providing greater versatility in the simulations, similarly to actual roots. The second computational scheme used is Reaction-Diffusion Root Branching (RDRB), which models the dynamic root growth using the finite element method (FEM) in 1D for the roots and 2D for the growing media. This model provides a more detailed and more complex description than the first one, considering the reaction-diffusion of the species, representing the biochemical search for nutrients. Additionally, it accounts for an elastic contribution to account for the mechanical effects of root growing and the media interaction. This model involves biochemical, biophysical, and tropism stimuli. The two proposed mathematical/computational models can correctly represent the plant root growth, incorporating geometrical aspects and biophysical and biochemical features. Furthermore, these models have the potential to be adopted to investigate other natural branching phenomena such as slime mold, fractures, circulatory systems, respiratory systems, and thunders.

Keywords: Growth algorithm, Root architecture, Root morphology, Computational simulation, Growth plant model.

Contents

List of Figures

List of Tables

Computational simulation and model of A generalized prototype of ornamental root.

XIII

Objectives

❖ Main objective

Identify the biological (evolutionary) and epigenetic process (due to the mechanical and biochemical environment) by which the growth of roots in plants happens to satisfy anchoring, support, and feeding processes. This is through computational simulation implementing phenomenological and reaction-diffusion models.

❖ Specific objectives

• Propose a mathematical and computational model to describe the branches of root plants under nutrient gradients and mechanical loads. This is through a phenomenological mathematical, and computational model of reaction-diffusion for nutrient gradients.

• Propose a mathematical and computational model to simulate different types of root morphologies in plants, considering the root architecture and tropisms.

• Propose a validation protocol for the computational model.

1. INTRODUCTION

Root archetypes

Leaves, stems, and roots are fundamental organs of plants. From those, the roots have a significant role because are they responsible for sustenance, anchorage, and water and nutrient absorption (Esau 1965; Taiz 2003; Gregory 2008; Eshel 2013; Glinski and Jerzy 2018). The study of different morphologies, behaviors, and adaptations are related to their functions are helpful to understand the biological development of plants (Esau 1965; Taiz 2003; Gregory 2008; Eshel 2013; Glinski and Jerzy 2018).

Different classifications have been proposed regarding the morphology n terms of genetic (Hochholdinger et.et al.,17) and topological features. The most common approach categorizes the morphologies as monocotyledonous and dicotyledonous (Eshel 2013; Glinski and Jerzy 2018). Another classification divides them into the adventitious and primary root, and from these, other root system archetypes can be defined as branching, fasciculate, and napiform (Figure 1) (Cannon 1949; Esau 1965). According to the previous classifications: Adventitious roots have many branches that emerge directly from the seed, e.g., the roots of maize. Primary roots have a unique principle a new root generation e.g., beans roots. Napiform roots as primary roots have a unique principal root, that behaves as an accumulator, e.g., carrots. Branching roots have a high density of branches regardless of the forms of the roots generations, and fasciculate roots have just one generation of branches that emerges from the seed.

Concerning the growth of the roots, the tendency that responds to a specific stimulus is called tropism, and it is relevant in the root development. Tropisms react to light,

gravity, anchoring, and chemical stimulus. They are typically referred to as phototropism, gravitropism, pleiotropism, and chemotropism, respectively (Esmon, et al. 2005; Met al.,a et.al. 20,11; Eshel 2013).
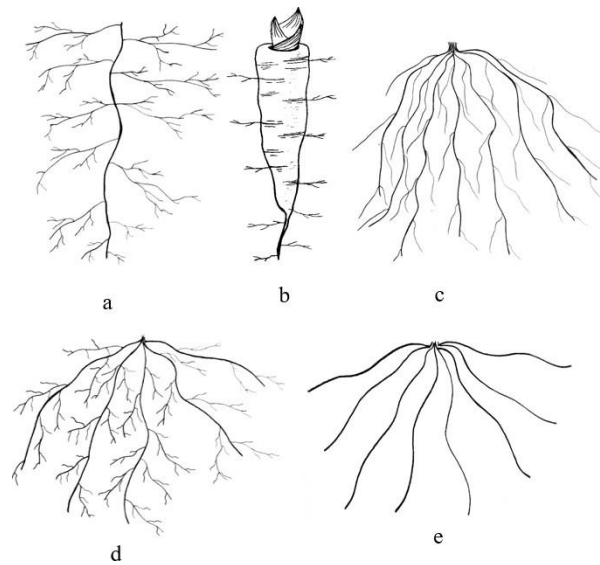
Figure 1. Drawings of some root system archetypes. a. Primary root, b. Napiform root, c. Adventitious root, d. Branching root and e. Fasciculate roots.

Some computational and experimental studies about root growth have been carried out (Popova et al., 2012; Fang et al., 2013; Adu et al., 2017; Bodner et al,. 2017). Experimentally, some researchers have identified environmental interactions (Clark, Whalley, and Barraclough 2003; Doussan, Pagès, and Pierret 2009; Walter, Silk, and Schurr 2009; Popova et al. 2012; de Moraes et al. 2018; Glinski and Jerzy 2018), intrinsic parameters, and growth patterns of roots using rhizoboxes(Youssef and Chino 1988) and image analysis software (Bodner et al. 2013; Fang et al. 2013; Aduet al. 2017). Rhizoboxes are employed to visualize and record the root development under the growing media e.g., the soil. Image analysis (French et al. 2009; Bodner et al. 2013; Pace et al. 2014) is used to understand the visual information, evaluating the photographic record, and obtaining growth data in real time. The main drawback in experimental methods is associated with cost and the time required to perform the test.

In general, these outcomes are used to design and validate mathematical root growth models.

1.2   Biophysics and biomechanics response

The biophysical analysis of cells in plants is affected by the pressure of turgor, shape, and movement as they grow. At the cellular level, the growth process changes and deforms the extracellular matrix. The turgor pressure is a differential in the osmotic potential inside and outside the cell, and it is in the range of 3 to 10 atm. The cell wall is a connected extracellular matrix made of cellulose, hemicellulose, pectin, other polysaccharides, and some structural proteins (Lise A, Kierzkowska R, Smith R, 2012).

Bidhendi A and Geitmann A (2018) suggest an approach to the biomechanical behavior of the cells, in which the cell wall has a deformable material, and the loads are given by turgor pressure, thus remark reversible and irreversible processes. From the above, the material has elastoplastic characteristics are underlined when taking it as hyperplastic. However, these assumptions must be reviewed since the results and conclusions of cell behavior depend significantly on elastoplastic features. Another option to understand this deformable material is to evaluate it from its plastic, elastic, or viscoelastic behavior. The behavior of the cells is elastic until reaching a certain threshold due to the forces caused by turgor pressure, and it is irreversible (Lise A, Kierzkowska R, Smith R, 2012).

The strength of root penetration happens by the resistance of the soil, different growth trajectories of nutrient and water searching, obstacles in the growth media, non-uniform conditions, and soil porosity (Kolb, 2017). The medium in which the roots grow can be natural soil, artificial soil, agar, and even water.

Roots elongate when the soil pressure exceeds soil mechanical impedance (Singh, 1998). Natural soil is particular for its texture (particle sizes) and composition. The heterogeneity of the media is relevant because, as the roots move, they reorganize

the soil particles changing the porosity of the soil. Homogeneity, humidity, and soil compaction are significant to identify the mechanical impedance of the growing media. The impedance is related to the growth trajectories that obey both tropisms and the search of resources (i.e., nutrients and water) (Kolb, 2017).

For the penetration of the root into the soil the following assumptions are taken: 1. The axial thrust is held produced by anisotropic cell growth driven by turgor. 2. Radial growth of the root tip reduces the axial resistance of the soil and stabilizes the root axis against buckling. 3. The reorientation of the root apex through passive and active mechanisms or differential growth in the different sections of the root. (Kolb, 2017).

According to mechanical stress, tension is weaker than compression stress. In a composite material approach, the soil can be understood as a matrix and the roots as a reinforcement. Roots are dependent on several variables, including the number of roots crossing potential shear planes, the strength and diameter distributions of those roots, and the orientation of roots with respect to the direction of the failure plane (Thomas, 2009).

1.3 Biochemical response

Auxin is the hormone that stimulates growth genes in stems, roots, and leaves. For example, in roots, there is a process of positive geotropism and negative phototropism (Figure 2). Inversely, the leaves and stem cells are elongated at low levels of auxin. The oscillation of auxin varies in different regions of the pericycle near or far from the apical meristem, this oscillation makes them susceptible to generating lateral roots. (It is due to a constant oscillation of auxin) (Eschel, Beeckman, Taiz) IAA (nature-3-acetic acid) low levels of auxin are necessary for root elongation, IAA is synthesized at the apex and transported at the root.
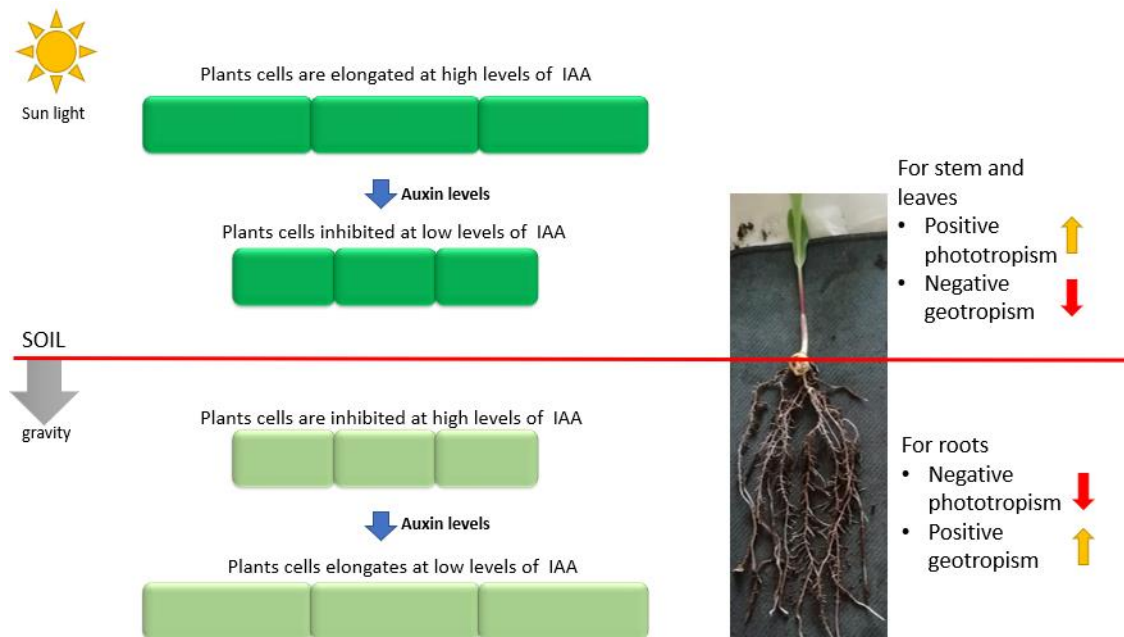
Figure 2. Scheme of tropism effects of sunlight (phototropism), gravity (geotropism), and auxin levels in cellular growth. Below the soil, the roots have negative phototropism, and positive geotropism, and the cells are elongated if the level of auxin hormone is low. The opposite happens with stems and leaves over the soil.

Auxin, as a plant-growth regulator, induces cell elongation because it increases the extensibility of the cell wall, by metabolic effects inside the cell. Additionally, it promotes the formation of lateral roots originated from small groups of cells in the pericycle, where auxin stimulates cells to divide. However, the election of the primary root is inhibited by auxin concentrations greater than 10-8 M (Taiz. 2002).

The nutrients found in the medium influence root growth and development; for example, the effect of nitrate and ammonium on the flow of auxin promotes the elongation of cells at the root (Ötvös et al. 2021). The root meristem activity and the elongation growth of the primary root are adjusted to optimize the supply of nutrients to the plant body, considering the availability of nutrients in the environment (López - Bucio et al, 2003). The adjustment of root growth dynamics in different nitrogen regimes depends on the precise modulation of auxin transport routes between the

bark and the epidermis (Ötvös et al. 2021). Also, water is another external factor in the environment since it is a promoter of the growth and development of the root.

Plant cell division can be understood as an interaction between auxin and cytokinin levels, being auxin an activator and cytokinin an inhibitor of auxin. Cytokinin directly affects the polarity of auxin and its effects on plant development. Cytokinin and auxin play an antagonistic role, an increase in one hormone inhibits the other one (Di Mambro, 2017).

Root growth is favorable in slightly acidic soils, with pH values between 5.5 and 6.5. The proliferation of roots depends on the availability of water and minerals in the immediate microenvironment surrounding the root (rhizosphere) (Taiz. 2002).

Within the soil, nutrients can move to the surface of the root by the flow of water. The amount of nutrients provided to the root depends on the rate of water flow through the soil to the plant, which depends on the rates of perspiration and the levels of nutrients in the soil solution (Taiz. 2002).

1.4 Computational models

A current alternative to study the root growth, the biophysical and biochemical effects is the use of computational and mathematical models. These models are defined in physical, biological, and mechanical aspects, and describe the root development applying statistical and mathematical analysis (Bodner et al. 2017). Computational models (Popova et al. 2012; Yang et al. 2013; Bodner et al. 2017; de Moraes et al. 2018; Pace et al. 2014; Boudon et al. 2015, Schleicher et al. 2015; Counede et al.) work to predict the growth patterns of different roots morphologies *in silico.* Previous studies have simulated the behavior of some root architectures (Fitter 1987; Lynch 1995; Godin et al. 1999; Doussan et al. 2009; Counede et al. Orman-Ligeza et al. 2014). Considering the root architecture as the features that describe branch lengths, radii, angles between branches, number of generations or branching order, and other intrinsic properties associated with tropisms. For example, the L-system model

(Leitner et al. 2010, Lynch 1995) simulates different root architectures centering on the root system and dynamic development. Other models include a morphological classification of roots applying statistical analysis (Bodner 2013). Besides, are other computational approach using FEM, most of them dealing with the mechanical properties of anchoring and the root-soil interaction when the root is pulled up from the media (Kolb 2017, Yang 2014, Kennaway 2019). Other computational models proposed an approach for simulating water uptake, and a root growth model upscaling from the individual single root level to the general complete root system (Wilderroter 2001).

1.5 Proposed Laboratory protocol

To validate the computational approaches is necessary experimental support. To this is used some protocols to check the growth of the roots. One of the most common experimental data to support these simulations is the seed cultivation in a controlled environment, and the image analysis using specialized software for root growth. In this section a laboratory protocol based on previous research is presented.

1.5.1 Aim

Identify different morphological growth characteristics in roots such as angles, growth velocity, number of branches, and branches generations (Bouma et al 2000, Clark et al 2011, Popova et al 2012, Bodner et al 2017). Corresponding data were used as parameters for the computational models and comparing the actual roots with the computational simulation.

1.5.2 Scope

This protocol describes one experimental procedure to obtain root characteristics. The procedure is about take pictures of the roots while are growing (terms of days), and subsequently using an analysis of images software to identify and obtain

characteristic data of the root growth (Clark et al 2011, Popova et al 2012, Bodner et al 2017). The roots must be in controlled environmental conditions (light, humidity, and temperature).

1.5.3 Target group

Students and researchers interested in the growth and simulation of the growth of roots in plants. The procedures were performed in the biomimetic laboratory of the National University of Colombia- Biotechnology institute.

1.5.4 Procedure

1.5.4.1 Equipment

- Incubator (light, humidity, and temperature control) (Figure 3).
- Camera.
- Stereoscopy
- Image analyzer software such as: RIA(ImageJ) (Lobet et al 2017), WinRHIZO (Pornaro et al 2017), saRIA (Narisetti et al. 2019) and RhizoVision (Seethepalli et al. 2021)

1.5.4.2 Reagents

- Culture medium: Agar
- Ethanol 70 %
- Hypochlorite 30 %
- Water
- Inorganic fertilizer NPK (Aziz et al 2020).
- Seeds of plants (corn, bean, carrot, orchid)

Note 1. Agar hydrogels (1% by weight), water at 80 °C and agar, the mixture it

must be constantly stirred until a homogeneous solution is achieved (Aziz et al 2020).

Note 2. The NPK fertilizer is prepared by the elucidation 1g of the fertilizer N:P:K (20: 5: 20) per 1L of distilled water (Aziz et al 2020).

Note 3. Seeds must be sterilized to prevent growth of microorganisms (Aziz et al 2020).

The media is prepared with Agar and NPK (fertilizer) in rhizoboxes of 20 x 40 x 2 cm in a glass of 1/8 inch thick and resistant to temperature. In the media are introduced germinated seeds at least 1 cm under the surface. These seeds must have a radicle approximately 2 cm in length. Then, rhizoboxes are in the boxes frame and departed in the incubator. (Aziz et al 2020).

The incubator has environmental conditions such as light, humidity, and temperature. The light must be white with ignition control, and time between 09:00 and 21:00 (150 mmol m-2s-1 radiation). Humidity must be at 40% and a temperature of 26 °C (air and water) during the completed germination. Then, after the germination, the plants are conserved between 10°C to 30 °C maximum. To check the technical data sheets and the literature about the environmental conditions and growth times for every type of plant is recommended (Aziz et al 2020).

1.5.6 Materials

- Rhizobox (Specialized boxes for root visualization) (Figure 3.)
- Camera holder (Figure 3.)
- Rhizobox holder (Figure 3.)
- Absorbent paper
- Petri dish

1.5.7 Protection elements

- Gloves
- Face masks
- Lab coat
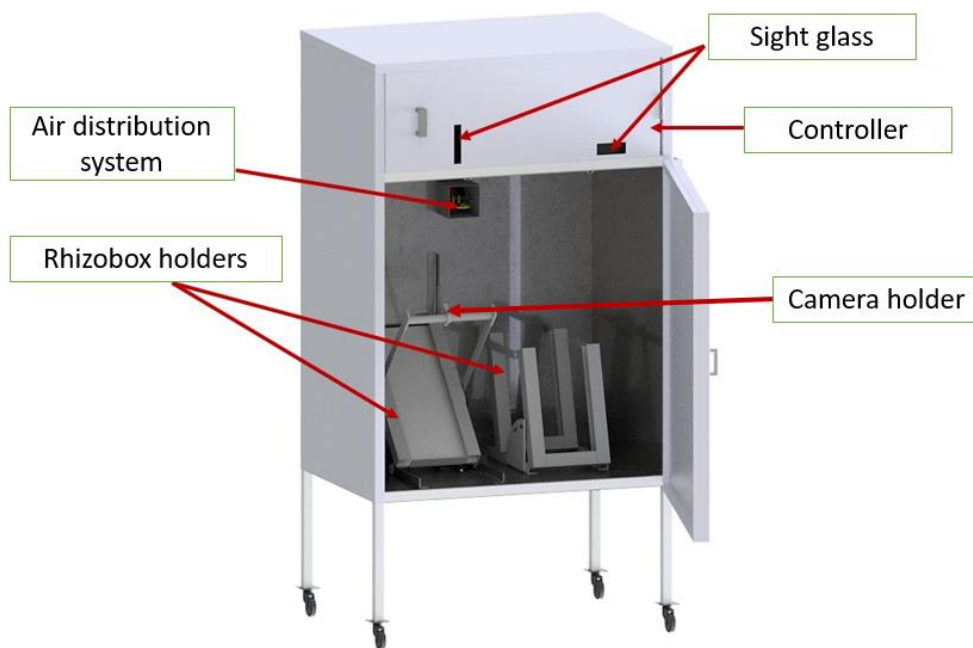
Figure 3. Assembly of the Rhizoboxes holders inside the Incubator

1.5.8 Seed germination procedure

For seed germination will be used paper method. For this are required two sheets of absorbent paper of 10 x 5 cm size. The seeds must be distributed uniformly over one of the sheets (Figure 4.a). Then seeds must be covered with the other sheet (Figure 4.b). The sheets of paper with seeds are folded and rolled up to locate inside the petri dish (Figure 4.c). The petri dish is closed and covered with aluminum foil to avoid light. Let the petri dish for 5 to 7 days, and then check the size of the primary root or radicle. When the radicle is 2 cm approximately (Figure 4.d), the seed will be retired from the

petri dish and located in the growth media within Agar and fertilizer.
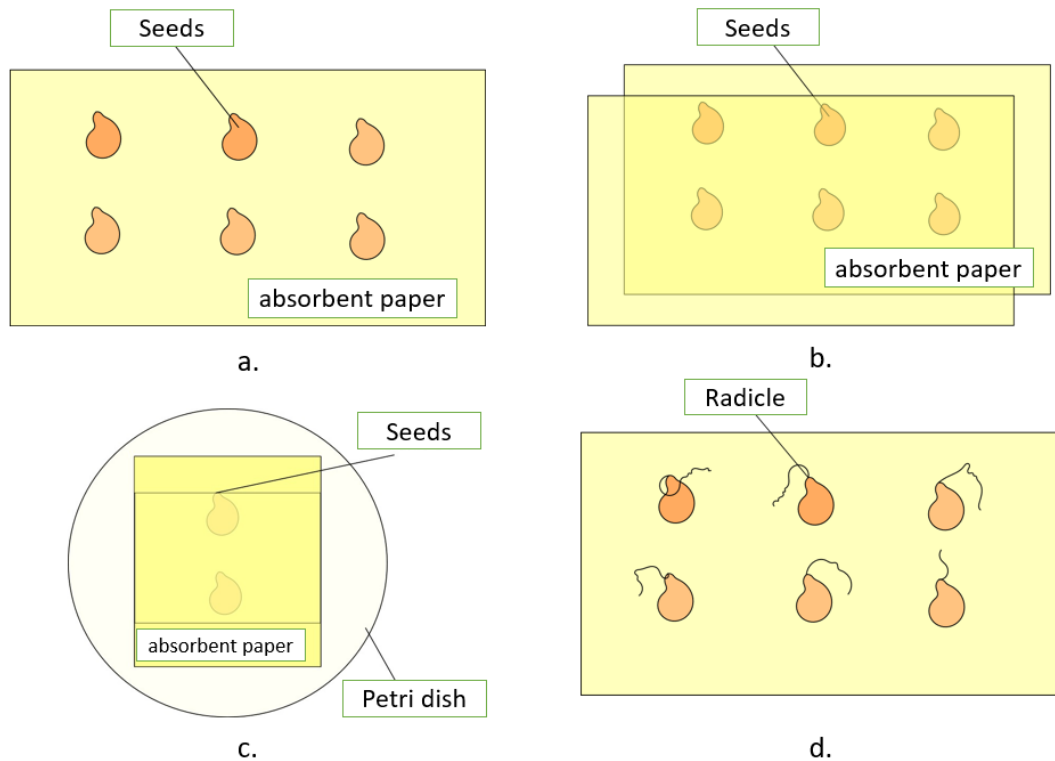
Figure 4. Germination of seeds. a. The seeds are distributed on the sheet of absorbent paper (10 x 5 cm), b. The seeds are covered with another sheet of absorbent paper, c. The sheets are rolled and folded with the seeds and arranged in a petri dish, d. After covering the petri dish to avoid light for 5 to 7 days, the radicle must be approximately 2 cm to give into the medium.

1.5.9 Image analysis

The camera holder will adjust the camera to a proper angle to take photographs every day (Clark 2013). The velocity of growth will take in mm per day. The photography will be saved on the computer to be uploaded in the image analysis software such as RIA(ImageJ) (Lobet et al 2017), WinRHIZO (Pornaro et al 2017), saRIA (Narisetti et

al. 2019), and RhizoVision (Seethepalli et al. 2021) to name few. Depending on the software tools and interface, are taken the parameters but in general are the same geometrical characteristics such as angles, length, the velocity of growth, and branches generations (Bouma et al 2000, Clark et al 2011, Popova et al 2012, Bodner et al 2017).

Computational simulation and model of A generalized prototype of ornamental root.

13

2. GROWTH ALGORITHM FOR THE COMPUTATIONAL SIMULATION OF ROOT MORPHOLOGIES IN PLANTS

In this chapter a computational model that, represents the dynamic root growth using stochastic, morphological, and tropism parameters are presented. These parameters have been taken from both literature and simulation. The model adopts the root system archetypes classification (Cannon 1949; Esau 1956; Eshel 2013; Taiz 2003) and involves a hybrid (biological-mathematical) approach. The background of the model is focused on the geometrical construction of the roots. For instance, can exemplify with greater geometrical accuracy the actual development of root archetypes configurations, namely: primary, adventitious, napiform, and fasciculate. The results of this investigation can be used to contrast complex studies related to the root system, and as a tool to guide researchers and students in areas of plant genetics, biological development of plants, root optimization for agriculture purposes, and biomimetic technological solutions inspired on plants morphologies.

2.1 Materials and methods

The proposed model considers a root as a sequence of segments growing in a Euclidean space. The branches of the root system are modeled using lengths and angles to simulate the tropisms and root system archetypes of a given species (Figure 1). The model uses global and local reference systems in both two and three dimensions. Growing root branches have been represented through time by an iterative process, beginning on the seed point where the root emerges and grow according to the plant species. Segments are modeled in n number of iterations, and time ranges from $t_1 = \Delta t$ to $t_n = \Delta t(n)$.

Segment creation scheme explained in Figure 5, starts from seed point (x_0, y_0, z_0) at time $t=0$. Later, segments have been developed by generations through a time interval of Δt. In the scheme, a new growing generation is shown in green. The blue vectors are about the first generation and green vectors are about the second generation. The α angle is according to the y-axis (vertical) and α_2 angle according to the x-axis (horizontal). The lengths are calculated at the end of each time step, where a new coordinate is assigned. This length will depend on the growing generation and algorithm type of root. The computational implementation of the described root model has been performed using MATLAB R19a. The model parameters are presented below and displayed in Table 1.

2.2 Model parameters

The model parameters have been obtained from the literature (Leitner et al. 2010; Bodner et al. 2013) and computational experimentation and are divided into three categories:

1.   Root intrinsic parameters, determined by the root system archetypes of each species. These are growth rate V_0 per generation, the number of generations N_g (branching order), and the relative angles (above which the next generations branches emerge) that defines the growth direction for the next generation of branches.

2.   Parameters given by root tropisms during plant development. These are growth angles in a coordinated space, where α denotes the angle on the x and y-axis, and γ the angle around the z-axis.

3.   Random factors (stochastic) that ensures the variability in the growth between plants of the same species when are modeled in different simulations. This stochasticity is necessary to represent morphological variations driven by genetics,

soil, and other factors we could not control on a simulation. Important concepts related with the model parameters introduced below.
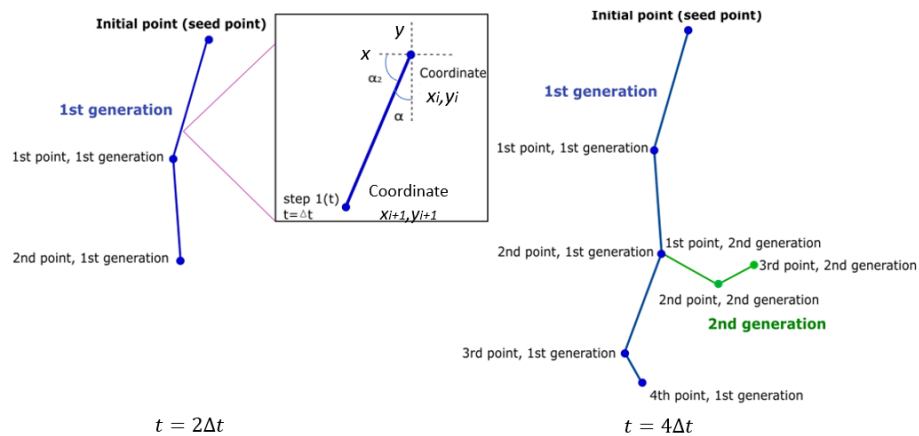
Figure 5. Segment creation scheme. Creation starts with the seed point, then by time steps, the growth is represented by segments and points with *x*, *y* coordinates. The segments can be of different generations (branching order)

- Seed: It is located at the coordinate system origin.

- Growth angle: As most of the branches grows in favor of gravity, the main growth is vertically descendant. However, some roots develop with a horizontal tendency for anchoring proposes (Eshel 2013) or resources uptake; in those cases, both the direction and angle depend on tropisms (Esmon et al. 2005; Miyazawa et al. 2011). On that line of though, the growth angle has been determined by the root system archetype, the tropism, and a random variable. Angle is different in each time interval. The value of the random variable has been assigned within a specific range, which varies according to the modeling plant.

- Generations: It is defined as the branching order from a specific root, divided in first, second, third generation. The number of generations depends on the

specie; for example, fasciculate roots usually have only one generation, different from primary root that have at least two generations.

- Growth rate: This growing speed is given for each generation, and it is a parameter of each root. A good example is the same primary root in which the growing speed of the main root is higher than the branches of the next generations.

- Branches: Branches can emerge from the seed or from other branches, according to corresponding generation. Each branch has an angle regarding the branch of the previous generation.

- Additional issues: In adventitious roots, the first and second generation emerges from the seed, and the first generation is longer than second. For primary roots, the first root generation grows faster than the other generations. In napiform, the first generation grows faster, and the radius are greater than the other generations. Finally, in fasciculate roots, the first generation has several branches that emerges from the seed.

2.2.1 Growth algorithm

The growth algorithm is a two and three-dimensional representation of root geometry. Angles and growth rates are associated with the model parameters of the algorithm (Figure 6, Appendix 1). In general, there are two stages, the first indicates the creation of the segment, and the second indicates the division of branches and generations per time iteration. The local and global systems are considering for both, two and three dimensions. The 3D systems incorporate a random angle around the z-axis at 360°.

The growth algorithm flow chart displayed in Figure 6, explains the model

parameters and the simulation conditions. Angles and growth rates indicate new branches, branch generations, and new coordinates. The first step at time $t_i = 1$ generates a new coordinate, as indicated by the dotted arrow. At times $t > 1$ branching by generations is evaluated before generating a new coordinate. The time advance defined by t_i, goes from $i = 1$ to $i = n$, the time interval defines by dt, and the total simulation time is $T = (n)dt$. This process is repeated for each time interval until the total simulation time ends. The division of a new branch of the same generation must satisfy, $V_s(i) < V_r$, where V_r is the growth rate generation assigned in the root model parameters. When these conditions are met, a new branch (or generation) is created. The information of the generation, branch number, coordinates and angles are stored. Both time step and length are dimensionless and consequently the growth rate can be modified a particular length or time step.
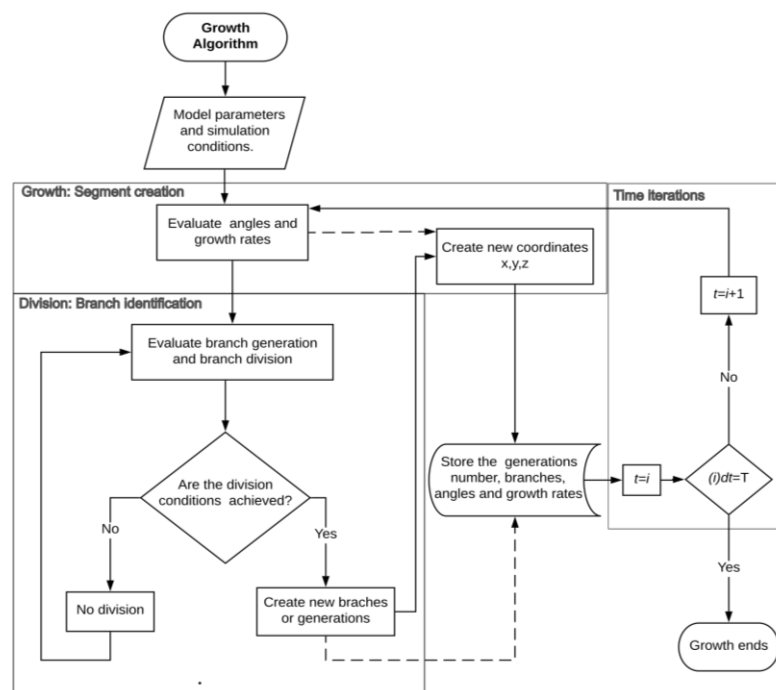
Figure 6. Growth algorithm flow chart. The first step is at time $t_i = 1$ generates a new coordinate, as indicated by the dotted arrow. At times $t > 1$ division by generations

or branches evaluates before generating new coordinates. The time advance is defined by t_i, which goes from $i = 1$ to $i = n$, the time interval defines by dt, and the total simulation time is $T = (n)dt$.

2.2.2 Simulation conditions

The simulation conditions are: total simulation time $T = t_n$, the time intervals Δt and the initial coordinates x_0, y_0, z_0.

Table 1: Computational parameters of root growth simulation. In the cases of study *Phaseolus vulgaris L* , *Zea mays*, *Phalaenopsis orchid*, and *Daucus carota* are indicated the growth rate and angle per root, according to the visual inspection of the roots.

Root system archetype	Primary	Adventitious	Fasciculate	Napiform
Simulation conditions				
Total simulation time (T)	100	100	100	100
Time interval (Δt)	1	1	1	1
Seed point location (x_0, y_0, z_0)	0,0,0	0,0,0	0,0,0	0,0,0
Root parameters				
Case of study	*Phaseolus vulgaris L*	*Zea mays*	*Phalaenopsis orchid*	*Daucus carota*
Growth velocity of the first-generation V ($l / \Delta t$)	4	2	0.1	4
Number of generations N_g	4	3	2	2
First generation angle (°)	180 a 185	180 a 185	220 a 225	180 a 185

Reference	Tested in Simulation	Leitner et al. 2010	Tested in Simulation	Tested in Simulation

2.3 Results and discussion

The versatility to modify and assign different root system archetypes is the most significant aspect of the developed root growth algorithm. In this way both, the simulation parameters and the time simulation can be adapted to reproduce a new root archetype. That is why the morphological root variations are consistently reproduced for the different simulations performed under the set of parameters and random conditions involved.

Four root system archetypes, i.e., adventitious, primary root, napiform, and fasciculate, have been simulated. Simulations are in two dimensions (2D) give a general idea of different root morphologies and allow an initial visual comparison with actual roots. Additionally, three-dimensional (3D) simulations allow a better spatial comprehension of the morphological development of the roots. Adventitious and primary roots were simulated in both 2D and 3D; napiform and fasciculate roots were just studied in 3D. In the spatial domain for roots, H indicates the total height (y-axis), A width (x-axis), and P depth (z-axis).

Is necessary to highlight that the numerical solutions are obtained according to the geometric architecture features of actual roots. In accordance, the visual inspection based on the aspect ratio between the branches is explored to validate the numerical results.

2.3.1 Simulations in 2D

2.3.1.1 Adventitious root

The 2D simulation for the adventitious roots, exemplified by a corn plant (*Zea Mays*),

offered the results displayed in Figure 7. Results have evidenced a radicular system with three generation of branches. Both the first (in orange) and second (in dark green) generations emerge from the seed point. The second generation starts growing in a horizontal direction, then it descends according to gravitropism behavior. The third generation (in light green) emerges horizontally along the second generations branches.

a.   *b.*
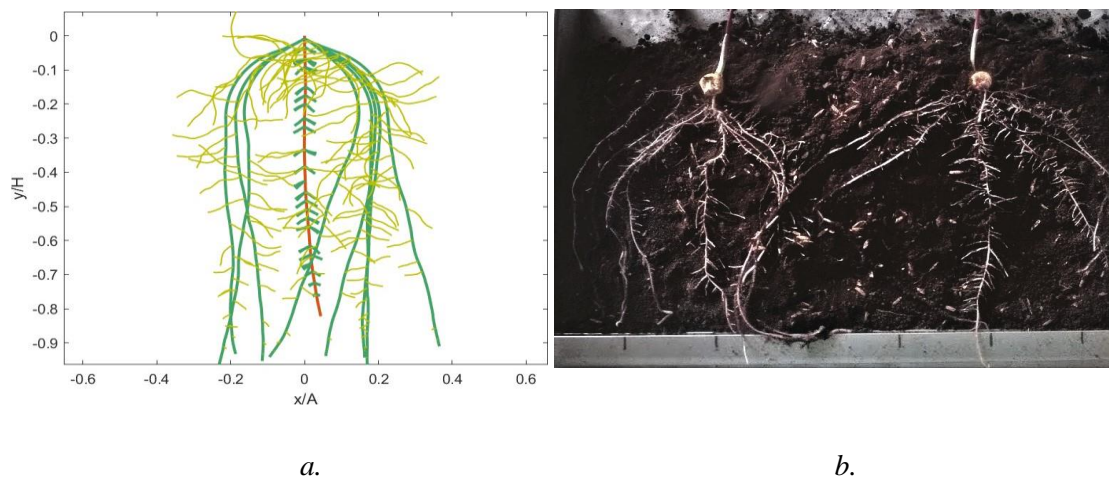
Figure 7. Adventitious root archetype. *a.* Simulation in 2D with three generations. *b.* Photography of actual root of *Zea Mays* after 10 days of growth.

According to simulation results, adventitious root arrangements have a significant similarity with other studies reported in the literature (Leitner et al. 2010), Bodner et al. 2013), and with actual roots (Figure 7 (b)). The parameters angles, rates, number of generations, lengths, and radius and the tropisms features are used to reproduce several root configurations.

It is possible to obtain different root arrangement for the same archetype, because of the stochastic variables of the model. It means, the input parameters and simulation conditions are the same, but the stochastic effect allows different configurations as is illustrated in the Figure 8.

Figure 8. 2D simulations of adventitious roots of *Zea Mays*. Figures *a, b, c,* and *d* illustrates different simulations applying the stochastic variables of the angle and using the same input parameters.

2.3.1.2 Primary root

The primary root archetype, exemplified in a common bean plant (*Phaseolus vulgaris L.*), has been simulated with a 2D growing model. Figure 9 presents correspondent results: the primary root (in orange) grows vertically according to gravitropism behavior. The second (in dark green) and third (in light green) root generations, grows horizontal according to pleiotropism behavior.
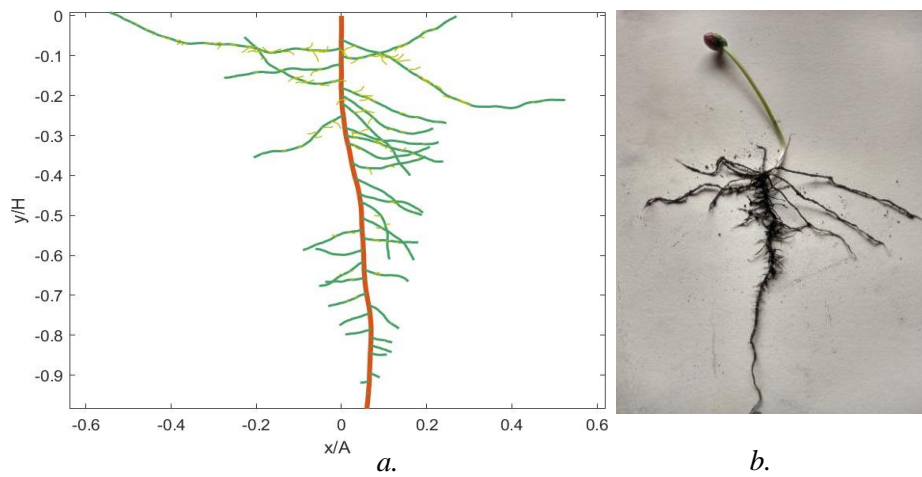
Figure 9. Primary root archetype. *a.* Simulation in 2D with three generations. *b.* Photography of actual root of *Phaseolus vulgaris L.* after 8 days of growth.

2.3.2 Simulations in 3D

2.3.2.1 Adventitious root

Adventitious root (*Zea Mays*) is represented in a 3D simulation in Figure 10. As the 2D simulation, the parameters of *x* and *y*-axis are the same, but the *z*-axis have a random angle for each time step.
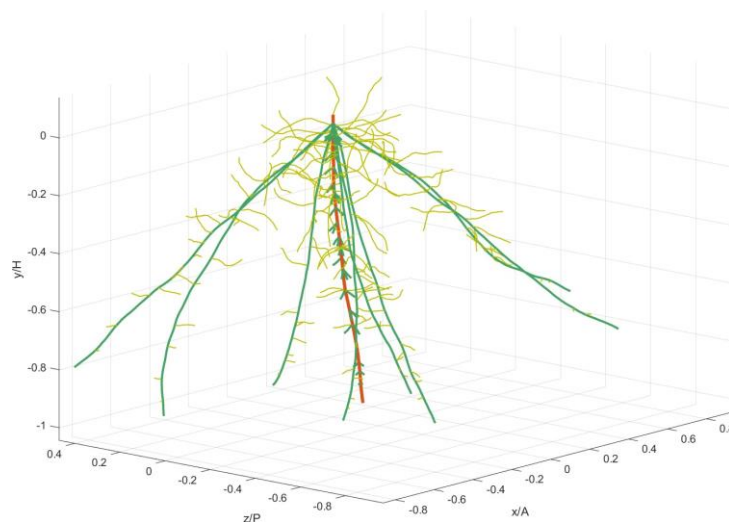
Figure 10. 3D simulation of adventitious root with three generations.

2.3.2.2 Primary root

The primary root 3D simulation in Figure 11, have the quite similar growth characteristics as the 2D simulation and, the *z*-axis has random angles for each time
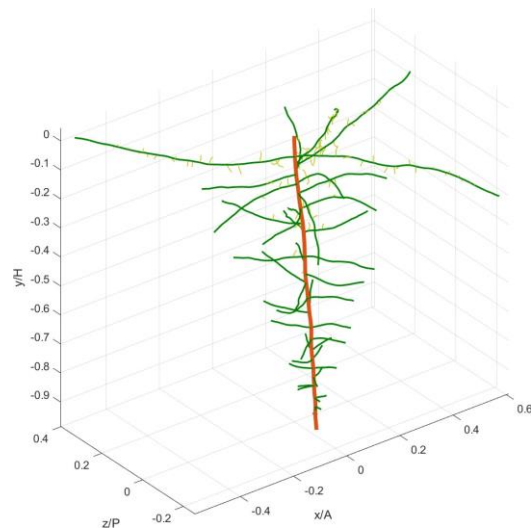
step.

Figure 11. 3D simulation of primary root with three different generations.

2.3.2.3 Napiform root

The 3D simulation of napiform root archetype, represented with a carrot plant (*Daucus carota*) (Figure 12), displayed a primary central root (in orange) having a larger radius comparing to the other archetypes. The subsequent generation grows horizontally, featuring by short and thin branches. As adventitious 2D results, is possible to obtain different root arrangement results from the same stochastic variables, parameters, and simulation conditions of the model, as seen in Figure 13.
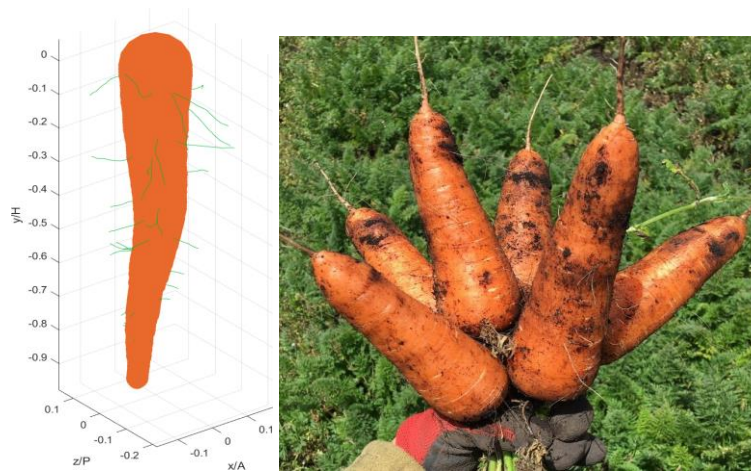
a.   *b.*

Figure 12. Napiform root archetype. *a.* 3D simulation of a napiform root, *b.* Photography of an actual napiform root.
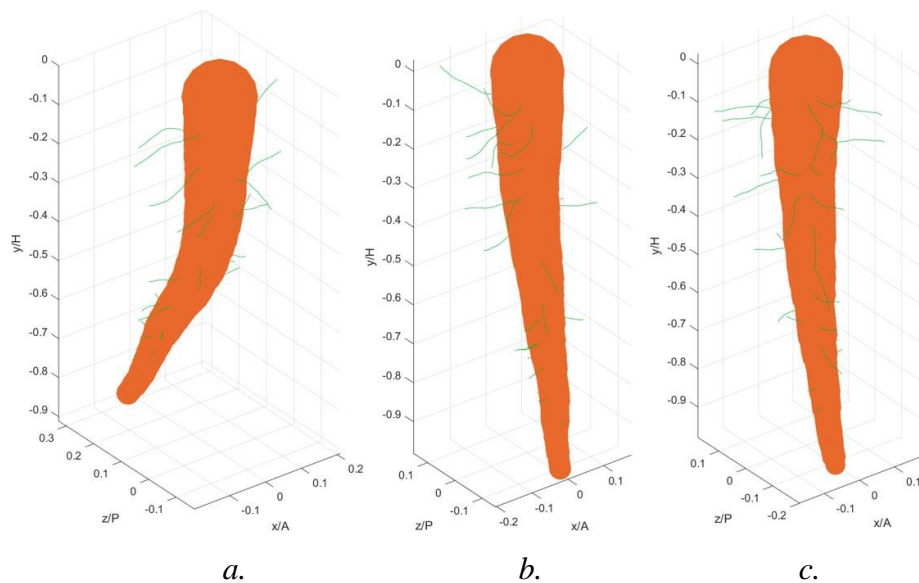
a.   *b.*   *c.*
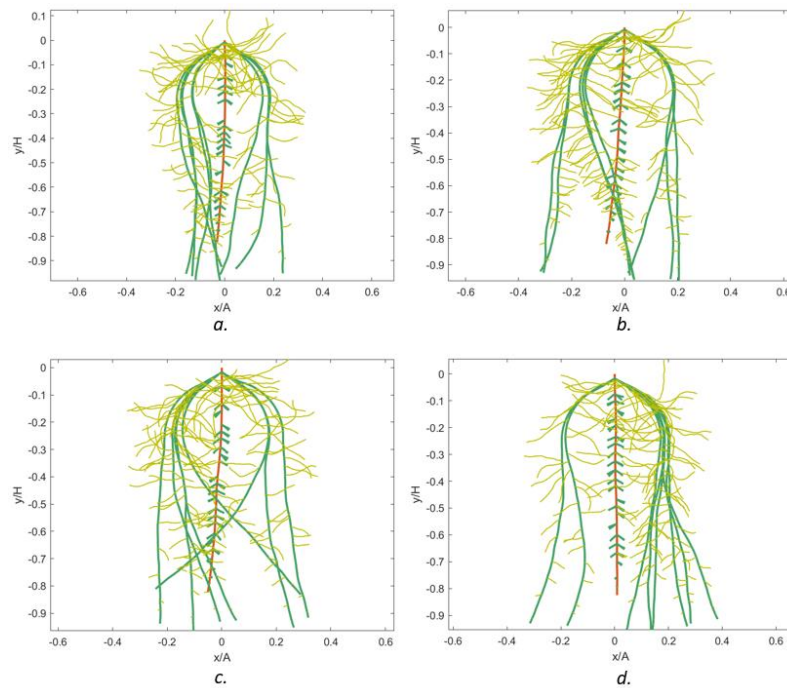
Figure 13. 3D simulations of napiform roots of *Daucus carota*. Figures *a, b* and *c* illustrates different simulations applying the stochastic variables of the angle and using the same input parameters.

2.3.2.4 Fasciculate root

The fasciculate root simulation in 3D, is sampled with an orchid plant *(Phalaenopsis orchid)* in Figure 14, presents a single generation (in green), which develops in both vertical (gravitational) and horizontal direction.

a.   b.
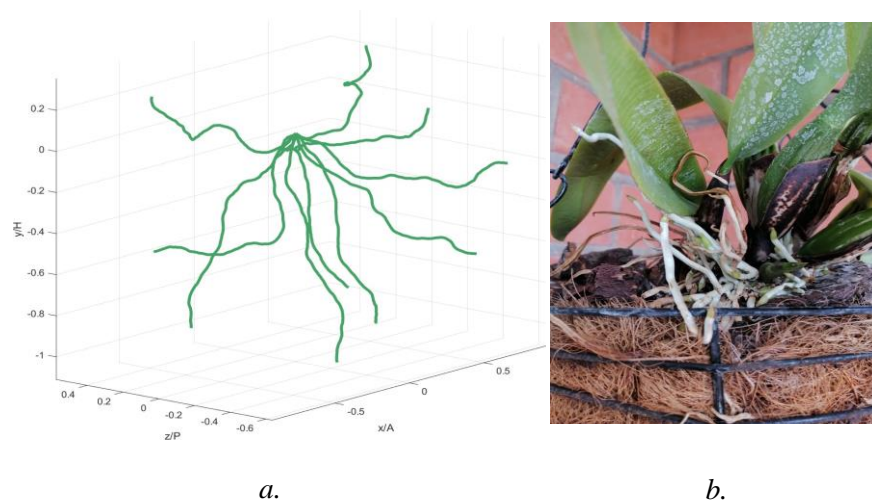
Figure 14. Fasciculate root archetype. *a.* 3D simulation of a fasciculate root, *b.* Photography of an actual fasciculate root

Further research can be undertaken to consider into the model environmental interactions, joining plant developing parameters concentration of nutrients, water supply, lighting effects, and obstacles into the media. Furthermore, it is possible to include mechanical analysis associating internal and external loading during the growth related to penetration, anchorage, and support of the root in the growing media.

2.4 Conclusions

The growth model based on root system archetypes helps study different architectures of the root system. The results reveal a similar appearance to existing

root systems due to both the use of stochastic variables and the versatility of the model.

The model's configuration permits analyzing the effect of tropisms and identifying geometrical features, helping to contrast complex studies related to morphological root development.

Despite currently several advanced computational software for root plant modeling, the alternative algorithm proposed in this paper can be easily improved by adding environmental interactions.

3   A COMPUTATIONAL MODEL OF ROOT GROWTH IN PLANTS, EMPLOYING FINITE ELEMENT METHOD IN UNIDIMENSIONAL SPACE AND REACTION-DIFFUSION MODEL.

In this chapter, a computational model RDRB (Reaction-Diffusion Root Branching) representing the dynamic root growth using the finite element method (FEM) is proposed. This new model considers a reaction-diffusion of Gierer-Meinhardt to represent the biochemical search of nutrients and an elastic model applying Hooke's equation to exemplify the mechanical effects of the growth and media interaction. The biochemical method is used to simulate the actual interaction between the root and the search for nutrients concentrated in the growing media. In addition, inside the root are a complex biochemical process that can be simulated with the reaction-diffusion models. For the biophysical approach, is used the elastic model describes the mechanical interaction between the growing media and the root, giving other growth criteria for the root branching. Both approaches in de model give an interesting approximation about the actual processes in the growth branching formations, contemplating the feed, anchoring and tropisms. The results of this investigation can be used to contrast studies related to the root system and future models for branching formations in different biological phenomena or even branching bio-inspiring applications.

3.1 Materials and methods

The root branching formations can be interpreted as a sequence of connected segments growing in the growing media and are stimulated by nutrient and water concentrations. Taking this into account, a mathematical model to represent root

branch formations using a finite element method was formulated in this work. The RDRB (Reaction-Diffusion Root Branching) model considers the following aspects: the reaction-diffusion response, branching angle, external stimuli of reaction-diffusion in the media, and mechanical external stimuli as schematically depicted in Figure 15. The model is simulated using a predetermined mesh of 1D elements for the root representation, and a 2D mesh of solid triangle elements for the media.

The RDRB model considers the following contributions:

E_D = Search of nutrients due to diffusion effects

E_R = Search of nutrients due to reaction effects

E_M = Mechanical effect of soil-root interaction per node, using mechanical characteristics of the media.

E_E = Search for external gradients applying the reaction-diffusion effects in the media.

E_a = Angle effect according to the tropisms, the angle effect used to restrict the other effects and is implicit in all the analysis.

The computational implementation of the described root model has been performed using ABAQUS, MATLAB 2019, and Gmesh software, and it can be described according to,

$$RDRB = (E_D + E_R) + E_M + E_E + E_{g.} \quad (1)$$

Is important to note the time discretization in the RDRB model. Discretization applies a Euler forward method. For the model, various single-time steps stabilize the reaction-diffusion response per node. For example, 50-time steps to declare a new generation of the root branching according to the reaction-diffusion internal (E_N) , external (E_E), and mechanical (E_M) stimuli.

3.1.1 Reaction - diffusion model

The reaction-diffusion model considered in this work is the Gierer-Meinhardt model (Eq. 2 and 3) (ref), defined in terms of activator parameter u, inhibitor parameter v, diffusion coefficients of activator Du, diffusion coefficients inhibitor Dv, and the reactive nonlinear functions of u and v, are f and g respectively (Eq. 4 and 5). The present formulation is discretized in time t using a Newton-Raphson method (ref).

$$\frac{\partial u}{\partial t} = D_u \frac{\partial^2 u}{\partial x^2} + f(u,v) \qquad \text{Eq. 2}$$

$$\frac{\partial v}{\partial t} = D_v \frac{\partial^2 v}{\partial x^2} + g(u,v) \qquad \text{Eq. 3}$$

$$f(u,v) = \rho \frac{u^2}{v} - \mu u + \rho u \qquad \text{Eq. 4}$$

$$g(u,v) = \rho u^2 - \mu_v v + \rho v \qquad \text{Eq. 5}$$

This RDRB model is applied for 1D and 2D finite element analysis considering external and internal stimuli. All mathematical solutions of Eqs. 2 and 3 are presented in Appendix 2.

3.1.2 Elastic model.

The elastic model is solved using the Hooke equation for elasticity (Eq. 6 and Eq. 7) applying the finite element method and solving with the Galerkin method,

$$\sigma = E\epsilon = E \frac{du}{dx} \qquad \text{Eq. 6,}$$

$$\nabla \sigma + b = \rho \frac{\partial^2 u}{\partial t^2} \qquad \text{Eq. 7.}$$

Using the Galerkin method and the weighting function of the finite element method. Is considered the elemental representation in Eq. 8,

$$\int_{\Omega^e} B \, \delta u. \, (DBu) d\Omega^e = \delta u \int_{\Omega^e} B^t \, DB d\Omega^e u. \qquad \text{Eq. 8}$$

Here, B is the matrix of weighting functions and matrix D is comprised by the material elastic constants, Young modulus E, and Poisson's ratio v.

The D matrix 3x3 is compound for:

$$D_{11} = D_{12} = \frac{E}{1-\nu^2},$$

$$D_{12} = D_{21} = \frac{\nu E}{1-\nu^2},$$

$$D_{33} = \frac{E}{2(1-\nu)}.$$

Mathematical solutions of the Eq.8 are indicated in Appendix 3.

3.1.3 Internal stimuli in 1D mesh

The RDRB growth model is developed by the connecting selected elements according to a reaction-diffusion analysis that also considers the branching angle. In this case, the angle must be higher than 180° due to the geotropism effect in the roots (Figure 15.b,15.c). The reaction-diffusion response is given in the element nodes, and they are geometrically restricted by a predetermined 1D mesh. All the elements connected to the same node are named as neighbor element, NE (Figure 15.a). Subsequently, the angle α between the nodes of these elements are calculated. In addition, the elements are selected for each time iteration (or time step) Δt, as illustrated in Figures 15.d and 15.c.
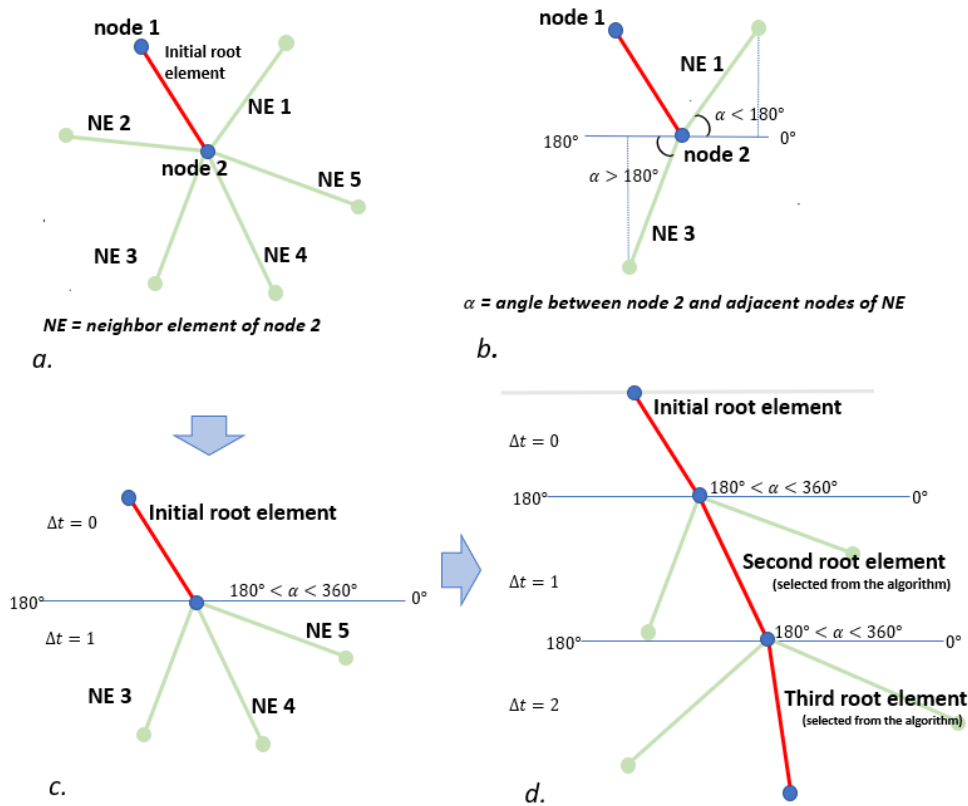
Figure *15*. Selection of elements in the 1D mesh. a) Initial root element and the NE of node 2. b) Angle α is measured between node 2 and the subsequent nodes of the NE, the selected element must be fulfilled that α > 180°. c) A new element must be selected after the time advance Δt =1 the possible elements are NE 3, 4, and 5 because of the α>180. d) Elements selected from time steps Δt =1 and Δt =2; elements are selected from the algorithm of the computational model.

3.1.4 External stimuli in 2D mesh

The solid mesh is made of triangle elements, the mesh nodes are equal to the nodes of the previous 1D mesh used in the root growth. The reaction-diffusion analysis is carried out in the mesh, and the analysis response is displayed by the nodes. The concentrations of both the activator *u* and the inhibitor *v* are quantified in the nodes, sharing information about the 1D mesh roots and the 2D external mesh. In consequence, the elements selected conform branches directed to sources of high concentration nodes of the 2D mesh.

3.1.5 Mechanical stimuli 2D mesh.

Mechanical stimuli are considered in the 2D mesh, applying an elastic analysis. The parameters for the model are the Poisson's ratio, Young modulus, and the load response per node. The boundary conditions are given by the load on the top of the soil mesh surface, and the displacement constraints are for *x* and *y* contours. The load applied in the negative *Y* direction. Furthermore, the root is used to grow where the load is lower and for the tropisms are always in the gravity direction (Figure 16).
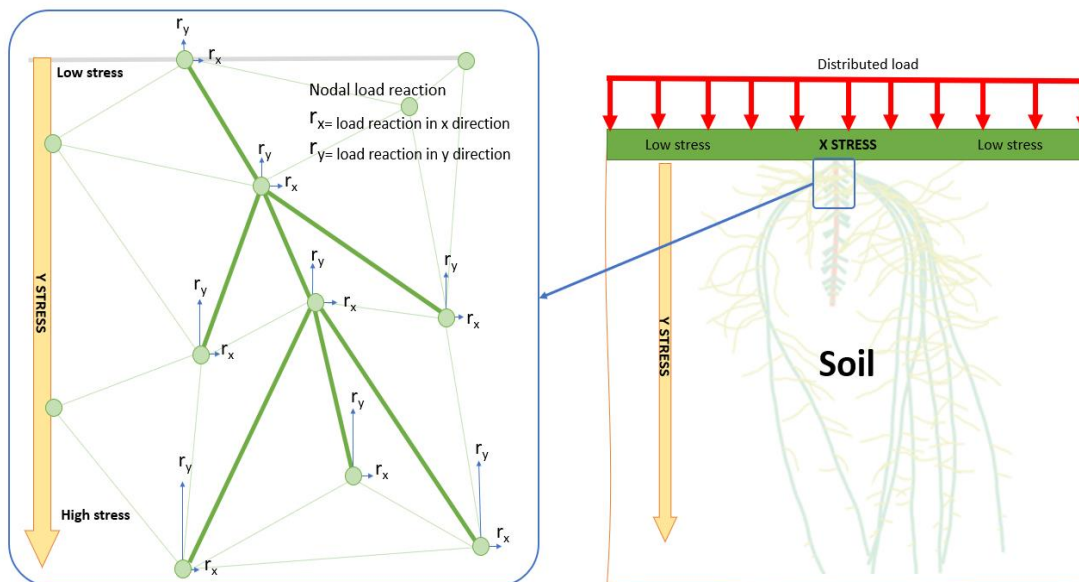
Figure *16*. Mechanical stimuli on the soil 2D mesh. The load response is evaluated per node, considering a mechanical analysis where the selected growing element corresponds to the nodes with the lowest load response.

3.1.6 Summary of model parameters

The summary of the parameters to obtain branching formations are as following: Branching angles α are between 180° and 360° for the geotropism and pleiotropism behavior. Reactive and diffusive constants γ (relative strength of the reaction terms) and D (ratio of the diffusive coefficients), are given the Turing patterns, but also can be determined for gradients auxins, cytokinin, and nutrient molecules. The mechanical

constants are the Poisson's ratio v= 0.3 and young modulus E = 1 MPa. For computational parameters, Δt is given by the forward Euler method.

3.1 Results and discussion

3.1.1 Mesh definition

Mesh construction is one of the most relevant facts in the simulation. Therefore, three different refinements and tested with the RDRB model for the 1D mesh are considered. In Figure 17 are illustrated the three branching examples, the coarse, medium and fine meshes respectively. For these meshes, the RDRB model analyze the angle, reaction-diffusion, and generates a new element per time step Δt.

a. Coarse mesh Nodes=45, Elements=112	*b.* Medium mesh Nodes=560, Elements=1597	*c.* Fine mesh Nodes=3009, Elements=8944
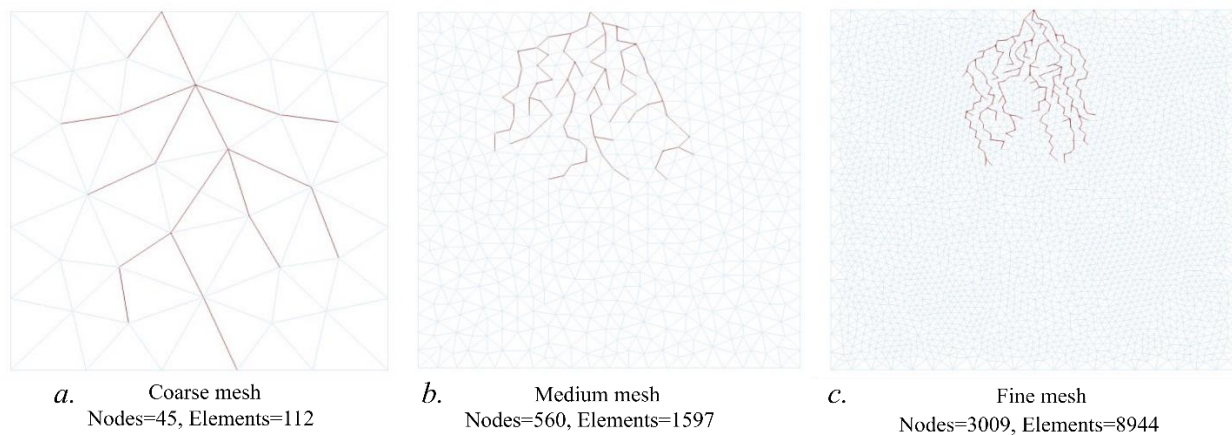
Figure *17*. Different resolution meshes applying RDRB model for 1D elements. a) coarse mesh, b) medium mesh, c) fine mesh.

The branching length, aspect ratio between the complete root and the branches, and angles are quite restricted by the initial mesh resolution and distribution. According the previous meshes is selected the medium mesh to simulate new tests, because of the computational cost.

3.1.2 Reaction-Diffusion effect

The reaction-diffusion effect in the RDRB model, is identify the node with the maximum concentration value of the activator agent to determine a new element. All

the nodes with more than one common element are used to have the maximum concentration of the activator agent.

For example, in the previous Figure 17 are selected as initial condition one element in the contour of the top to start the root, and the following branches are selected by the RDRB model for 1D mesh. Other example is illustrated in the Figure 18, for 1D mesh, but using as initial condition a predefined branching form, here the reaction-diffusion model generates subsequent branches in the predefined branching form.

a. Predefined branching form.

b. Simulation with the initial predefined branching form

Medium mesh. (Nodes=560, Elements=1597)
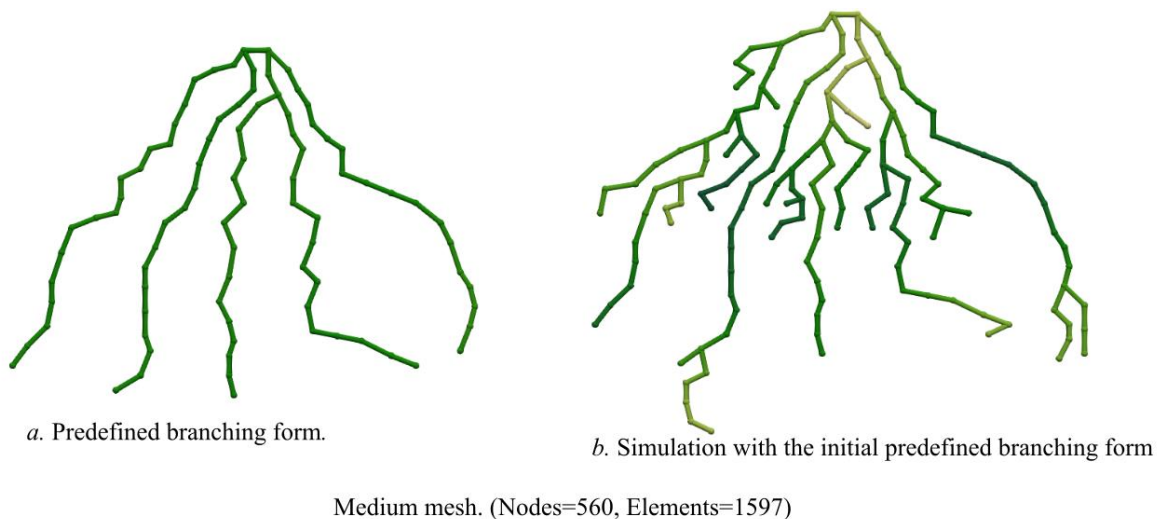
Figure *18.* Simulation using a). Predefined branching form as initial condition b). Emerging branches after simulating the RDRB model.

For internal (1D mesh) and external (2D mesh) reaction-diffusion in the RDRB model, the effect is applied in the nodes with the influence both high activator agent concentrations of external and internal stimuli. For example, in Figure 19 is illustrated in red a high concentration for the internal stimuli in the1D mesh, and in dark yellow the high concentration for the external stimuli (the growing media) in the 2D mesh. The model tends to select elements in the side of the mesh with the external higher concentrations.
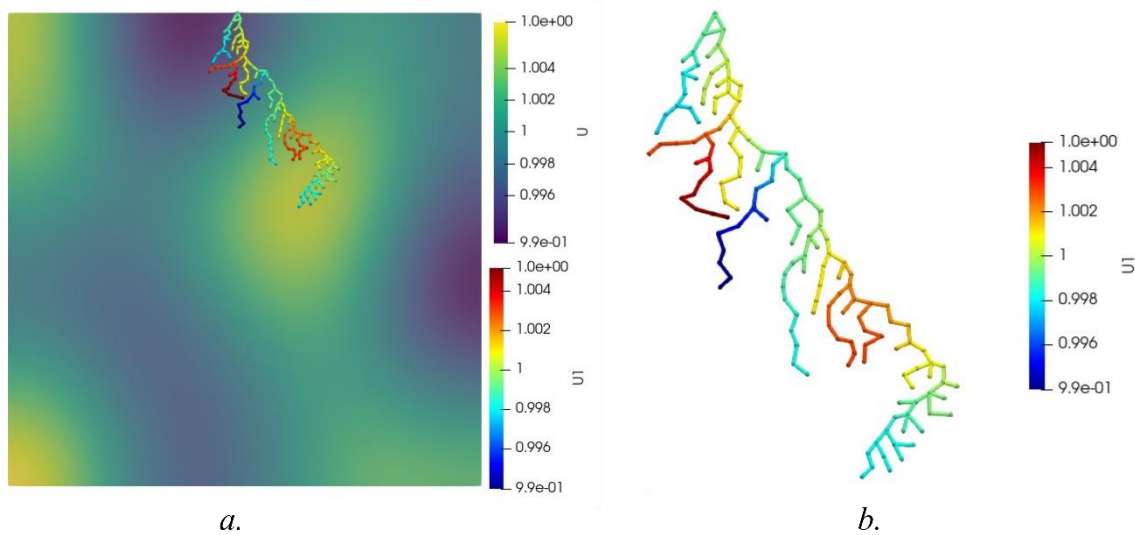
Figure 19.   Simulation of root branching formation in fine mesh (see Figure 17), according to the high concentration of the activator agent (e.g., nutrients, water.) in the growth media (2D Mesh), the angled influenced by geotropism and the internal reaction-diffusion.

3.1.3 Mechanical effect.

For the mechanical effect of the media, we apply an elastic analysis on the 2D mesh. The results are reported in the nodes of meshes 1D and 2D. For instance, the mechanical response is equal for the media and root.   As general computational experimentation is developed a simple test of mechanical effect using:

1) Boundary conditions: contour in the bottom and the left side is fixed and is applied a load of 1 in a positive Y direction on the superior contour;

2) Parameters: Poisson's ratio 0.3 and dimensionless Young modulus =1. As illustrated in Figure 20, the stress in the *x* direction is 0.3 equal to the Poisson's ratio and in the *y* direction is the applied load.

The parameters can be modified using actual biophysical parameters and boundary conditions of the media or roots.

Stress in Y direction   Stress in X direction

a   *b*
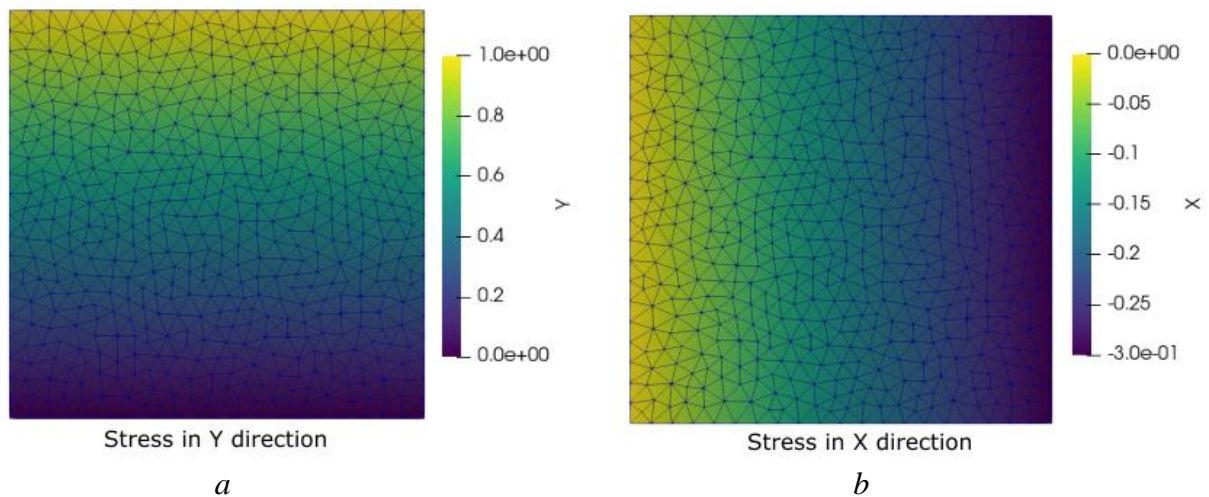
Figure 20. Stress in *y* and *x* direction. Boundary conditions are fixed on the bottom and left contour of the mesh. The load is applied in the superior contour of the mesh in a negative *y* direction. a) Stress result of the mesh in *y*-axis, the maximum value in the contour is the applied load, and for b) result of the mesh in *x*-axis, the maximum value (in *x* negative direction) is the Poisson's ratio. A media mesh is used in this simulation (see Figure 17)

3.1.4 Parameter characterization

To identify the influence of the parameters in the simulations is proposed a characterization comparing the number of elements generated, the media length of the contours, the maximum possible elements (one element per time step) and branching formations. For these tests are used the parameters in the Table 2.

Table 2. Simulation parameters to compare effects in the root growth using de RDRB model.

Parameters		Units
Number of iterations (Δt)	420	time
Box length (L_b)	1	Length
Elements per contour (Ce)	20	
$L_p = L_b/Ce$	0,05	Length

Ratio elements per time steps	420	Elements/time
Relative strength of the reaction terms (γ)	29	
Ratio of the diffusive coefficients (D)	10	
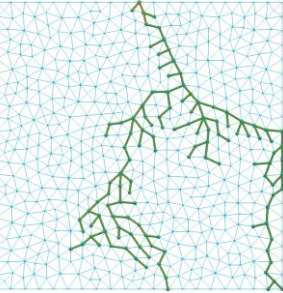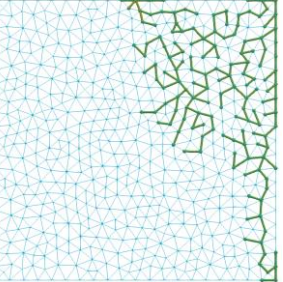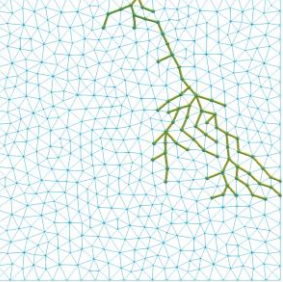
Characterization parameters are: the number of individual branches with three or more elements connected (N_b), the number of total elements connected in the root (N_e), the maximum vertical elements divided by the number of elements per contour (L_a), the equivalent length or all connected elements (L_{eq}), Total elements divided by the ratio of elements per iteration (T_{esp}).
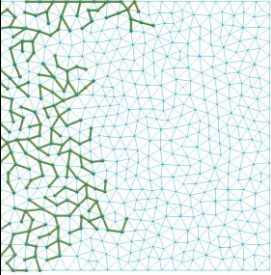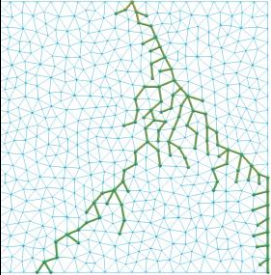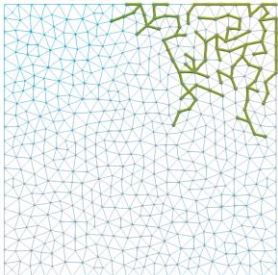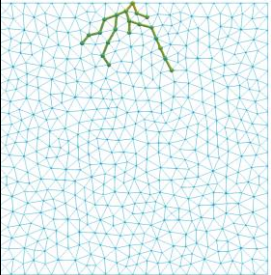
The assumptions in the simulations are:

1. The elements are contained in a finite domain, and it is possible restraint the element selection.
2. The external stimuli and internal (Diffusion + Reaction) can generate a new element per iteration (two different elements per iteration).
3. The angle condition is given if the internal or external stimuli select a node.
4. A new element per generation can be selected; however, in some iterations the conditions are not met.

Table 3. Branching simulation results using different configurations of parameters. For the simulations is used a medium mesh (see Figure 17)

Simulation		Diffusion	Reaction	External stimuli	Angle
1		x	-	x	x
2		x	-	x	-
3		x	-	-	x

4		x	-	-	-
5		x	x	x	x
6		x	x	x	-
7		x	x	-	x
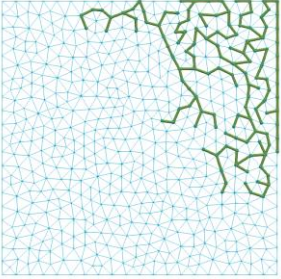
8		x	x	-	-

Table 3. Characterization of tests according to the number of elements per root, mesh, and steps time of the simulation.

Test number	Diffusion	Reaction	Ext. Stimuli	Angle	N_e	N_B	L_a	$\frac{N_e}{teps}$(%)	L_{eq}
1	x		x	x	120	9	1	28,57	6
2	x		x		148	12	1	35,24	7,4
3	x			x	72	8	0,75	17,14	3,6
4	x				193	25	1	45,95	9,65
5	x	x	x	x	109	12	1	25,95	5,45
6	x	x	x		91	9	0,50	21,67	4,55
7	x	x		x	19	3	0,25	4,52	0,95
8	x	x			131	12	0,70	31,19	6,55

According to Table 2. The angle is necessary to restrict the morphology and the tropism of root plants. Complementary, in Table 3, the reactive internal effect in the model is the most restrictive parameter. In test 4, applying only the diffusion, the

highest formation of branches and elements per iteration is obtained with 46% of the possible elements. The length L_a wish means that the root is at the bottom of the domain, and L_{eq} is also the maximum because of the maximum N_e. Comparing the presence and absence of the angle is restrictive but, the reactive effect is in a greater way more restrictive if the two effects are applied (test 7), the element selection of the root is at least 41% lower than the test 4. However, if the external stimuli are activated (test 5) the number of elements is improved by 21%. On the other hand, test 6 shows a reduction of the branches and Ne due to the finite domain, which is not possible with the selection of neighbor elements.

In summary, the internal and external diffusive stimuli promote the selection of new elements in the root simulation. In contrast, the reactive and the angle stimuli restrict the selection of new possible elements and allow the root morphology. The combination of external and internal reaction-diffusion, angle, and even the mechanical effect is an interesting approximation to represent root branching formations. On the other hand, the mechanical effect is not very significant in the simulation and is not considered in Tables 2 and 3.

3.2.5 Time step stabilization

Furthermore, is developed a test applying twenty and fifty iterations to select a new element. It means the search for the minimum or maximum concentration can have an equilibrium.

In Figure 21, the root branching is given by the unique effect of the internal diffusion with a restrictive angle of 225 to 315 degrees. Figure 21. a is constructed every 20 iterations, in the total time the root is longer than the Figure 21.b simulation with 50 iterations per element selection.
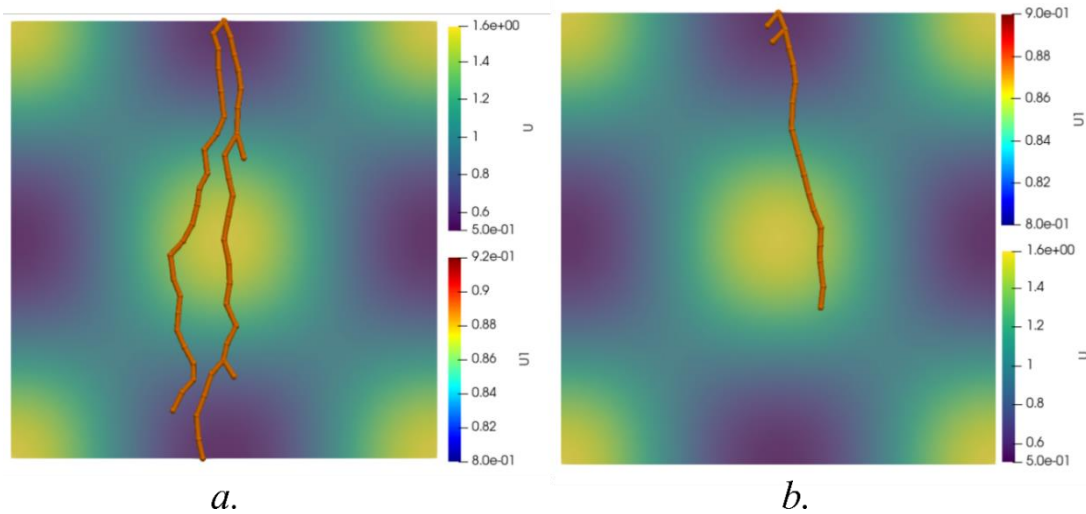
Figure 21. Simulations without reactive internal effects in a media mesh (Figure 17), total iterations = 9999. $D = 250$, $\gamma = 10$. a) Element selection every 20 iterations. b) Element selection every 50 iterations.

Figure 22 illustrates a simulation applying all the reaction-diffusion effects (external and internal) and the angle restriction of 180 to 360 degrees in response to the geotropism. For the total iterations, the element selection stopped at 3000 iterations. It is because the mesh (media height) is restrictive to choose another element. According to this simulation, is tested a new simulation with a new refined mesh.
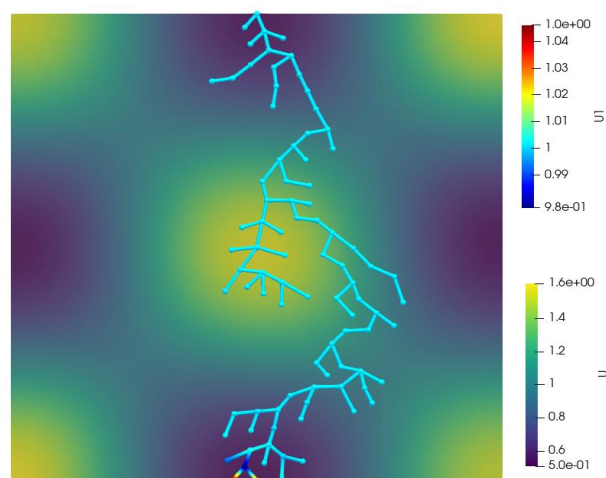
Figure *22.* Simulations without reactive internal effects, total iterations = 4800. D=250, γ=10, 50 iterations per element selection. A media mesh is used in this simulation (Figure 17).

In figure 23, is illustrated a new simulation with 3187 iterations, an element selection every 50 iterations and a fine mesh. Here, the root branching formation can grow continuously, and the effects of reaction-diffusion orientate the branches. The light green spots in the media (activator agent concentration U) are the nutrient sources. Furthermore, like geotropism, the angle restriction shows a vertical tendency.

a   *b*
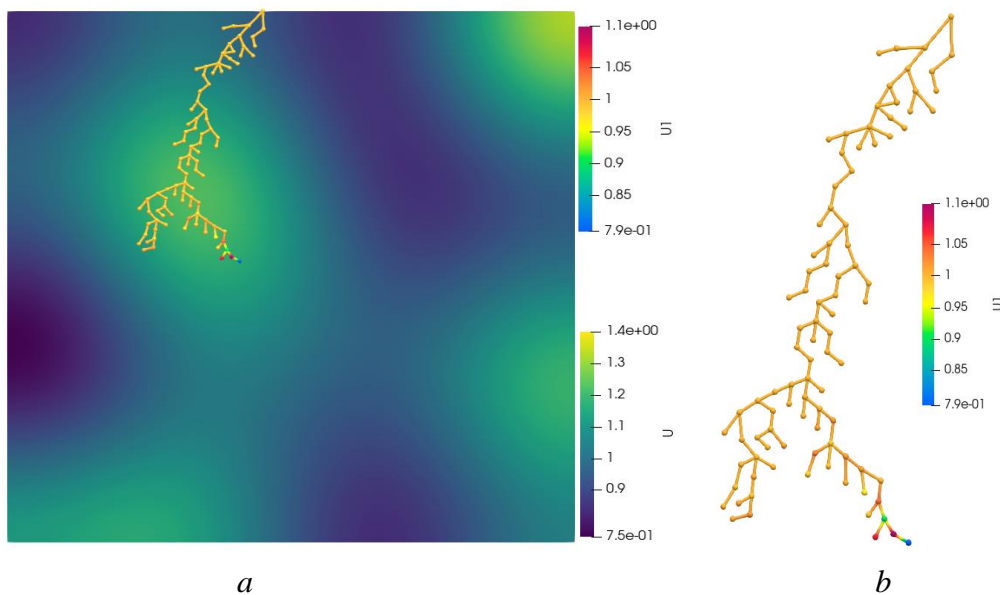
Figure *23.* Simulations without reactive internal effects, total iterations = 3187. D=250, γ=10, 50 iterations per element selection. It used a fine mesh (see Figure 15). a) Simulation with growing media (2D mesh) and root (1D mesh), b) simulation of root (1D mesh)

3.3 Conclusions

- The proposed RDRB model applying FEM has an interesting approach to simulating branching formations as the root plants with the biochemical (reaction-diffusion analysis) and biophysical (elastic analysis) stimulus.

- Only using an intermedia mesh in a finite domain, but non-specific parameters of nutrients concentration and mechanical properties are obtained a branching formation like the roots. However, the angle of root growth is always obeying geotropism.

- The reactive internal effect and the angle between 180° and 360° are more restrictive with the branching formations than the others.

- The internal diffusive effect and the external stimuli improve the branching formations if the reactive and the angle are restrictive.

- The mechanical analysis is applied in the model but is not changed in the tests. For instance, it is considered for future works.

3.4 Future work

- Apply to the model parameters of reaction-diffusion internal and external, mechanical properties of the soil, and different external loads for specific plants.

- Apply the proposed validation protocol

- Simulate the cell growth of the root.

- The model can be applied to other applications which require branching formations in biologists such as the slime mold, fractures, circulatory systems, respiratory systems, and thunders.

4. CONCLUDING REMARKS AND RECOMMENDATIONS

The two models have an attractive approach to simulate root growth. The first geometrical model reveals a similar appearance with actual root archetypes systems due to the stochastic variables and the versatility of the algorithm.

The second model RDRB illustrates a relevant branching formation as the root plants using a biochemical and biophysical approach with the reaction-diffusion and the elastic model respectively. These attributes to the model a complete background about the external and internal biophysical effects of the growth in roots.

The favorable mesh for the RDRB model is the intermediate mesh, due to the element lengths, and the computational cost.

As a future work is necessary to implement the validation protocol proposed in the document to validate the results of the root archetypes, and the soil-root interactions.

A recommendation for the RDRB model is to include parameters of reaction-diffusion internal and external, mechanical properties of the soil, and different external loads using actual information of plants. Finally, validate with image analysis the root archetypes and simulations.

The computational model for root morphologies to include the effect of external parameters as obstacles that can affect the geometrical distribution of roots is recommended. Eventually, validate with image analysis the root archetypes and simulations.

5.REFERENCES

Adu, M. O., Yawson, D. O., Bennett, M. J., Broadley, M. R., Dupuy, L. X., and White, P. J. (2017). A scanner-based rhizobox system enabling the quantification of root system development and response of brassica rapa seedlings to external p availability. Plant Root, 11,16–32. https://doi.org/10.3117/plantroot.11.16.

Aziz, A. A., Lim, K. B., Rahman, E. K. A., Nurmawati, M. H., & Zuruzi, A. S. (2020). Agar with embedded channels to study root growth. Scientific Reports, 10(1), 1-12

Bentley, L. P., Stegen, J. C., Savage, V. M., Smith, D. D., von Allmen, E. I., Sperry, J. S., and Enquist, B. J. (2013). An empirical assessment of tree branching networks and implications for plant allometric scaling models. Ecology letters, 16(8), 1069-1078.https://doi.org/10.1111/ele.12127.

Bodner, G., Alsalem, M., Nakhforoosh, A., Arnold, T., and Leitner, D. (2017). RGB and spectral root imaging for plant phenotyping and physiological research: Experimental setup and imaging protocols. Journal of Visualized Experiments, 2017(126). https://doi.org/10.3791/56251.

Bodner, G., Leitner, D., Nakhforoosh, A., Sobotik, M., Moder, K., and Kaul, H. P. (2013). A statistical approach to root system classification. Frontiers in Plant Science, 4(AUG).https://doi.org/10.3389/fpls.2013.00292.

Boudon, F., Chopard, J., Ali, O., Gilles, B., Hamant, O., Boudaoud, A., .and Godin, C. (2015). A computational framework for 3D mechanical modeling of plant morphogenesis with cellular resolution. PLoS Comput Biol, 11(1), e1003950. https://doi.org/10.1371/journal.pcbi.1003950.

Boyer, J. S., Silk, W. K., & Watt, M. (2010). Path of water for root growth. Functional

Plant Biology, 37(12), 1105-1116. Bouma, T. J., Nielsen, K. L., & Koutstaal, B. A. S. (2000). Sample preparation and scanning protocol for computerised analysis of root length and diameter. Plant and soil, 218(1), 185-196.

Cannon, W. A. (1949). A tentative classification of root systems. Ecology, 542-548. https://doi.org/10.2307/1932458

Clark, L. J., Whalley, W. R., and Barraclough, P. B. (2003). How do roots penetrate strong soil? Plant and Soil (Vol. 255). https://doi.org/10.1007/978-94-017-2923-9 10.

Clark, R. T., MacCurdy, R. B., Jung, J. K., Shaff, J. E., McCouch, S. R., Aneshansley, D. J., & Kochian, L. V. (2011). Three-dimensional root phenotyping with a novel imaging and software platform. Plant physiology, 156(2), 455-465.

Cournède, P. H., Kang, M. Z., Mathieu, A., Barczi, J. F., Yan, H. P., Hu, B. G., and De Reffye, P. (2006). Structural factorization of plants to compute their functional and architectural growth. Simulation, 82(7), 427-438. https://doi.org/10.1177/0037549706069341¨ı.

de Moraes, M. T., Bengough, A. G., Debiasi, H., Franchini, J. C., Levien, R., Schnepf, A., and Leitner, D. (2018). Mechanistic framework to link root growth models with weather and soil physical properties, including example applications to soybean growth in Brazil. Plant and Soil, 428(1–2), 67–92. https://doi.org/10.1007/s11104-018-3656-z

Doussan, C., Pagès, L., and Pierret, A. (2009). Soil exploration and resource acquisition by plant roots: An architectural and modelling point of view. In Sustainable Agriculture (pp. 583–600). Springer Netherlands. https://doi.org/10.1007/978-90-481-2666-8-36. Esau, K. (1965). Plant anatomy. Plant Anatomy., (2nd Edition).

Dowdy, R. H., Smucker, A. J. M., Dolan, M. S., & Ferguson, J. C. (1998). Automated Image Analysis for Separating Plant Roots from Soil Debris Elutriated from Soil Cores. In Root Demographics and Their Efficiencies in Sustainable Agriculture, Grasslands and Forest Ecosystems (pp. 737-744). Springer, Dordrecht.

Eshel, A., and Beeckman, T. (Eds.). (2013). Plant roots: the hidden half. CRC press.

Esmon, C. A., Pedmale, U. V., and Liscum, E. (2005). Plant tropisms: Providing the power of movement to a sessile organism. International Journal of Developmental Biology. https://doi.org/10.1387/ijdb.052028ce

Fang, S., Clark, R. T., Zheng, Y., Iyer-Pascuzzi, A. S., Weitz, J. S., Kochian, L. V., . . . Benfey, P. N. (2013). Genotypic recognition and spatial responses by rice roots. Proceedings of the National Academy of Sciences of the United States of America, 110(7), 2670–2675. https://doi.org/10.1073/pnas.1222821110.

Fitter, A. H. (1987). An architectural approach to the comparative ecology of plant root systems. New phytologist, 106, 61-77. https://doi.org/10.1111/j.1469-8137.1987.tb04683.x

French, A., Ubeda-Tomás, S., Holman, T. J., Bennett, M. J., and Pridmore, T. (2009). High-throughput quantification of root growth using a novel image-analysis tool. Plant physiol- ogy, 150(4), 1784-1795. https://doi.org/10.1104/pp.109.140558

Gliński, J., and Lipiec, J. (2018). Soil physical conditions and plant roots. CRC press.

Godin, C., Costes, E., and Sinoquet, H. (1999). A method for describing plant

architec-ture which integrates topology and geometry. Annals of botany, 84(3), 343-357.

Gregory, P. J. (2008). Plant roots: growth, activity and interactions with the soil. JohnWiley & Sons. Hochholdinger, F., Yu, P., and Marcon, C. (2018). Genetic control of root system development in maize. Trends in plant science, 23(1), 79-88.

Hodge, A., Berta, G., Doussan, C., Merchan, F., and Crespi, M. (2009). Plant root growth, architecture and function. Plant and soil, 321(1), 153-187. https://doi.org/10.1007/s11104-009-9929-9.

Leitner, D., Klepsch, S., Knieß, A., and Schnepf, A. (2010). The algorithmic beauty of plant roots–an L-System model for dynamic root growth simulation. Mathematical and Computer Modelling of Dynamical Systems, 16(6), 575-587. https://doi.org/10.1080/13873954.2010.491360

Lobet G, Koevoets IT, Noll M, Tocquin P, Meyer PE, Pagès L, et al. Using a structural root system model to evaluate and improve the accuracy of root image analysis pipelines. Front Plant Sci. Frontiers; 2017;8. doi:10.3389/fpls.2017.00447

Lynch, J. (1995). Root architecture and plant productivity. Plant physiology, 109(1), 7. https://doi.org/10.1104/pp.109.1.7

Miyazawa, Y., Yamazaki, T., Moriwaki, T., and Takahashi, H. (2011). Root Tropism. Its Mechanism and Possible Functions in Drought Avoidance. Advances in Botanical Research (Vol. 57). https://doi.org/10.1016/B978-0-12-387692- 8.00010-2.

Narisetti, N., Henke, M., Seiler, C., Shi, R., Junker, A., Altmann, T., & Gladilin, E. (2019). Semi-automated root image analysis (saRIA). Scientific reports, 9(1), 1-10.

Orman-Ligeza, B., Civava, R., de Dorlodot, S., and Draye, X. (2014). Root system architecture. In Root engineering (pp. 39-56). Springer, Berlin, Heidelberg. https://doi.org/10.1007/978-3- 642-54276-3 3

Popova, L., Russino, A., Ascrizzi, A., and Mazzolai, B. (2012). Analysis of movement in primary maize roots. Biologia, 67(3), 517–524. https://doi.org/10.2478/s11756-012-0023-z.

Pornaro, Cristina & Macolino, Stefano & Menegon, Alessandro & Richardson, Mike. (2017). WinRHIZO Technology for Measuring Morphological Traits of Bermudagrass Stolons. Agronomy Journal. 109. 10.2134/agronj2017.03.0187.

Schleicher, S., Lienhard, J., Poppinga, S., Speck, T., and Knippers, J. (2015). A method-ology for transferring principles of plant movements to elastic systems in architecture. Computer-Aided Design, 60, 105-117. https://doi.org/10.1016/j.cad.2014.01.005.

Seethepalli, A., Dhakal, K., Griffiths, M., Guo, H., Freschet, G. T., & York, L. M. (2021). RhizoVision Explorer: Open-source software for root image analysis and measurement standardization. bioRxiv.

Taiz, L. and Zeiger, E. (2003). Plant physiology. 3rd edn. Annals of Botany, 91(6), 750–751.

Walter, A., Silk, W. K., and Schurr, U. (2009). Environmental Effects on Spatial and Temporal Patterns of Leaf and Root Growth. Annual Review of Plant Biology, 60(1), 279–304. https://doi.org/10.1146/annurev.arplant.59.032607.092819

Yang, M., Defossez, P., Danjon, F., and Fourcaud, T. (2014). Tree stability under wind: simulating uprooting with root breakage using a finite element method. Annals of botany, 114(4), 695-709. https://doi.org/10.1093/aob/mcu122.

Youssef, R. A., and Chino, M. (1988). Development of a new rhizobox system to studythe nutrient status in the rhizosphere. Soil Science and Plant Nutrition, 34(3), 461–465. https://doi.org/10.1080/00380768.1988.10415701.

6. APPENDIX

1. Growth Algorithm

Growth Algorithm

% (a) Model parameters: Growth rate (*V*), growth angles *α* for plane *X-Y* and *γ* for Z axis, Numberof generations (*Ng*), Initial shape of root (*Fi*) Growth rate for any root morphology.

% b) Simulation conditions: time interval (Δt), Total time t_n, seed point (x_0, y_0, z_0)

1: Initialize parameters

2: x=0; y=0; z=0   *%Coordinates seed point*

3: *Ng*=k;   *%k is the number of generations*

4: *Nr*=nr;   *%nr is the maximum number of branches per generations*

5: *V*=a;   *%a is the grow rate per any k generations*

6: *n=T*;   *%T is the total time of simulation*

7: *dt=t*;   *%t is the time interval in the simulation*

8: *h*=+-15;   *%Variable range of 15 degrees*

9: *α*(1) =270+rand(*h*);   *%gravity direction (270 degrees) and variable random amount in h range*

10: Define and initialize coordinates

11: *x=V* (1) *cos(*α*(1))

12: *y=V* (1) *sin(*α*(1))

13: **for** i=1:n **do**   *% Time counter per generation*

14:     **for** g=1:nr **do**   *% Branch counter per generation*

15:          *α*(i+1)=*α*(i)+rand(h)

16:          *x*(i+1) =*x*(i)+ V*cos(*α*(i))

17:          *y*(i+1) =*y*(i)+ V*sin(*α*(i))

18:          Vs(i)=((x(1) $-x$(i))^2 +(y(1) $- y$(i))^2)$^{1/2}$ %*Vs is the rate calculated in the simulation*

19: Flag to generate a new generation

20:          **if** *rand > 5 & V* (*g*) > *V s*(*i*) & *t > i* **then**

21:　　　　　　　*generation*(*i*)=1 *%Branches for the new generation is created*

22:　　　**else**

23:　　　　　　　*generation*(*i*)=0 *%Branches for the new generation cannot be created*

24:　　　**end if**

25: Flag to generate a new branches of the same generation

26:　　　　*Vr(g)*=j % j is the growth rate of branches of the same generation

27:　　　**if** $V\,s(i) > V\,r(g)$ **then**

28:　　　　　　　*div $\_$rama*(*i*)=1; *%If is equal to 1, branches are created*

29:　　　**else**

30:　　　　　　　*div $\_$rama*(*i*)=0; *%If is equal to 0, branches cannot be created*

31:　　　**end if**

32:　　**end for**

33: **end for**

2. Gierer-Meinhardt Reaction-diffusion model formulation.

$$\frac{\partial u}{\partial t} = D_u \frac{\partial^2 u}{\partial x^2} + f(u, v)$$

$$\frac{\partial v}{\partial t} = D_v \frac{\partial^2 v}{\partial x^2} + g(u, v)$$

D_u y D_v are diffusion constants for activator substance u, and inhibitor substance v

$$f(u, v) = \rho \frac{u^2}{v} - \mu u + \rho u$$

$$g(u, v) = \rho u^2 - \mu_v v + \rho v$$

Using wighted residuals,

$$\int_\Omega = (\frac{\partial u}{\partial t} - D_u \frac{\partial^2 u}{\partial x^2} - f(u, v))W_u d\Omega = Ru$$

$$\int_\Omega = (\frac{\partial v}{\partial t} - D_v \frac{\partial^2 v}{\partial x^2} - g(u, v))W_v d\Omega = Rv$$

Following the equations (9) and (10)

$$R_u = \int_\Omega w_u \frac{\partial u}{\partial t} d\Omega - \int_\Omega \frac{\partial w_u}{\partial x} \frac{\partial u}{\partial x} d\Omega - \int_\Omega w_u f(u, v))d\Omega$$

$$R_v = \int_\Omega w_v \frac{\partial v}{\partial t} d\Omega - \int_\Omega \frac{\partial w_v}{\partial x} \frac{\partial v}{\partial x} d\Omega - \int_\Omega w_u g(u, v))d\Omega$$

Galerkin standard, $U = N^T U \; and \; W = C^T N$

$$R_u = \int_\Omega C^T N \frac{\partial N^T u}{\partial t} d\Omega - \int_\Omega \frac{\partial C^T N}{\partial x} \frac{\partial N^t u}{\partial x} d\Omega - \int_\Omega C^T N f(u,v)) d\Omega$$

U is *t* dependent, and *N* is *x* dependent.

$$R_u = C^T \int_\Omega N N^T \frac{\partial u}{\partial t} d\Omega - C^T \int_\Omega \frac{\partial N}{\partial x} \frac{\partial N^T}{\partial x} d\Omega u - C^T \int_\Omega N f(u,v)) d\Omega$$

$$\int h(x) dx = \sum_{i=1}^{n} h(x_i) w_i$$

Applying shape functions. Local coordinates in ξ space (linear elements of 2 nodes)

$$x = N_1 x_1 + N_2 x_2$$
$$x = N_1(\xi) x_1 + N_2(\xi) x_2$$
$$N_1 = \frac{x_2 - x}{x_2 - x_1} = \frac{1 - \xi}{2}$$
$$N_2 = \frac{x - x_1}{x_2 - x_1} = \frac{1 + \xi}{2}$$

Formulation using ξ space.

$$R_u = \int_\Omega N N^T J d\xi \frac{\partial u}{\partial t} - \int_\Omega \frac{\partial N}{\partial x} \frac{\partial N^T}{\partial x} J d\xi u - \int_\Omega N f(u,v)) J d\xi$$

Temporal advance is given by finite differences, and Newton- Raphson method

$$f'(x_0) \Delta x = -f(x_0)$$

$$Ru = M_u \frac{u^{t+\Delta t} - u^t}{\Delta t} + k_u u^{t+\Delta t} - F$$

$$Rv = M_v \frac{v^{t+\Delta t} - v^t}{\Delta t} + k_v v^{t+\Delta t} - G$$

$$\begin{bmatrix} \dfrac{\partial Ru}{\partial u} & \dfrac{\partial Ru}{\partial v} \\[4mm] \dfrac{\partial Rv}{\partial u} & \dfrac{\partial Rv}{\partial v} \end{bmatrix} \begin{bmatrix} \Delta u \\[2mm] \Delta v \end{bmatrix} = \begin{bmatrix} -Ru \\[2mm] -Rv \end{bmatrix}$$

Solving,

$$\frac{\partial Ru}{\partial u}\Delta u + \frac{\partial Ru}{\partial v}\Delta v = -Ru$$

$$\frac{\partial Rv}{\partial u}\Delta u + \frac{\partial Rv}{\partial v}\Delta v = -Rv$$

$$\frac{\partial Ru}{\partial u^{t+\Delta t}} = \frac{Mu}{\Delta t} + Ku - \frac{\partial}{\partial u^{t+\Delta t}}(F)$$

$$\frac{\partial Ru}{\partial v^{t+\Delta t}} = -\frac{\partial}{\partial v^{t+\Delta t}}(F)$$

$$\frac{\partial Rv}{\partial u^{t+\Delta t}} = \frac{\partial}{\partial u^{t+\Delta t}}(G)$$

$$\frac{\partial Rv}{\partial v^{t+\Delta t}} = \frac{Mv}{\Delta t} + Kv - \frac{\partial}{\partial v^{t+\Delta t}}(G)$$

Convective or reactive nonlinear terms.

$$F = \int Nf(u^{t+\Delta t}; v^{t+\Delta t})Jd\xi$$
$$G = \int Ng(u^{t+\Delta t}; v^{t+\Delta t})J$$

3. Elastic formulation finite element.

The elastic model is solved using the Hooke equation for elasticity applying the finite element method and solving with the Galerkin method, where $\sigma = E\epsilon$; $\sigma = E\dfrac{du}{dx}$.

$$\nabla \sigma + b = \rho \frac{\partial^2 u}{\partial t^2}.$$

Using weighted residuals,

$$R_\Omega = A(\dot{u}) - A(u); \int_\sigma w R_\Omega \, d\Omega = 0.$$

Elemental Galerkin equation.

$$\int_{\Omega e} \left(w\left(\nabla \cdot \sigma(\epsilon(u))\right) + b - \rho \frac{\partial^2 u}{\partial t^2}\right) d\Omega = 0$$

Strong form, there w is the weight function.

$$\int_{\Omega e} w\left(\nabla \cdot \sigma(\epsilon(u))\right) d\Omega^e + \int_{\Omega e} wb \, d\Omega^e - \int_{\Omega e} w\rho \frac{\partial^2 u}{\partial t^2} d\Omega^e = 0$$

Weak form, applying Green-Stokes theorem.

$$-\int_{\Omega e} \frac{\partial w}{\partial x} \cdot \sigma \, d\Omega^e + \int_{\Omega e} wb \, d\Omega^e - \int_{\Omega^e} w\rho \frac{\partial^2 u}{\partial t^2} d\Omega^e + \int_{\Gamma e} w\sigma \cdot n \, d\Gamma^e = 0$$

For the weak form, the term $\int_{\Omega^e} \frac{\partial w}{\partial x} \cdot \sigma \, d\Omega$ is the same as the double dot product between the

tensors $\int_{\Omega e} \left(\frac{\partial w}{\partial x}\right)^S : \sigma \, d\Omega + \frac{\partial w^\alpha}{\partial x} : \sigma \, d\Omega$, and representing an asymmetric and symmetric

according the weight function, $\nabla w = \frac{1}{2}\nabla w + \frac{1}{2}\nabla w + \frac{1}{2}\nabla w^T + \frac{1}{2}\nabla w^T = \frac{1}{2}(\nabla w + \nabla w^T)$.

In summary the elemental elastic equation is given by

$$\int_{\Omega^e} \nabla w : o \, d\Omega^\epsilon + \int_{\Omega^e}^{wb} d\Omega \, e - \int_{\Omega^e} w\rho \frac{\partial^2 u}{\partial t^2} d\Omega^e + \int_{\Gamma e} w\sigma \cdot n \, d\Gamma^e$$

The approximation functions are given by the shape function *N* and depends on the element type. E.g., triangle elements could have three *N* functions (*N1, N2, N3*), and the square could have four *N* functions *(N1, N2, N3, N4).* For triangle element type are,

$$u = N1(x)u1 + N2(x)u2 + N3(x)u3 \, ,$$

$$\delta u \ = \ N1(x)c1 \ + \ N2(x)c2 \ + \ N3(x)c3 \, .$$

The equation in the weak form, can be expressed as:

$$\int_{\Omega e} B\delta u \cdot (DBu) d\Omega^e - \delta u \int_{\Omega e} B^T DB \, d\Omega^e \, u$$

Where $B = \mathcal{L}N$, $B^T = \mathcal{L}N^T = \nabla N^T$, and $\mathcal{L}$ is:

$$\mathcal{L} = \begin{bmatrix} \dfrac{\partial()}{\partial x} & 0 \\[2mm] 0 & \dfrac{\partial()}{\partial y} \\[2mm] \dfrac{\partial()}{\partial y} & \dfrac{\partial()}{\partial x} \end{bmatrix}$$

D is the matrix with the mechanical parameters Young modulus, and Poisson's ratio.

$D11 = D22 = \dfrac{E}{1-v^2}$, $D12 = D21 = \dfrac{vE}{1-v^2}$ and $D33 = \dfrac{E}{2(1-v)}$

$$D \ = \ \begin{bmatrix} D11 & D12 & 0 \\ D21 & D22 & 0 \\ 0 & 0 & D33 \end{bmatrix}$$

In terms of shape functions N, the weak form equation is given by:

$$\int_{\Omega e} \nabla N \cdot D \nabla N^T \, d\Omega^e \, u + \int_{\Omega e} \rho N^T N \, d\Omega^e \frac{d^2 u}{dt^2} = \int_{\Omega^e} N^T b \, d\Omega^e + \int_{\Gamma e} Nn\nabla u d\Gamma^e$$

The weak form can be equivalent to this equation $r = M\dfrac{d^2 u}{dt^2} + Ku - F - BC,$

Where, $M\dfrac{d^2 u}{dt^2} + Ku$ is the rigid matrix, *F* is the force vector and *BC* is the boundary conditions.

For time discretization the finite differences using Euler forward method is applied. Given by $\dfrac{\partial Ru}{\partial u}\Delta u + \dfrac{\partial Ru}{\partial v}\Delta v = -Ru$, and $\dfrac{\partial Rv}{\partial u}\Delta u + \dfrac{\partial Rv}{\partial v}\Delta v = -Rv$. Where u and v are displacements.